International Journal of Sediment Research xxx (xxxx) xxx

Contents lists available at ScienceDirect

International Journal of Sediment Research

journal homepage: www.elsevier.com/locate/ijsrc

Original Research

Physical and chemical characterization of sediments from an Andean river exposed to mining and agricultural activities: The Moquegua River, Peru

Luis de Los Santos Valladares [a, *], Juan Luis Ccamapaza [b], Renato Arturo Valencia-Bedregal [c], Luis Enrique Borja-Castro [c], Jose Velazquez-Garcia [a], Dehiwalage Harshani Nimalika Perera [a], Adrian Ionescu [a], David Arvidsson [a], Eustace Peregrine Barnes [a], Peter Newton [a], Hugo Lepage [a], Patrick Byrne [d], Angel Guillermo Bustamante Dominguez [c], Crispin H.W. Barnes [a]

[a] Cavendish Laboratory, Department of Physics, University of Cambridge, Cambridge CB3 0HE, United Kingdom
[b] Escuela Académico Profesional de Ingeniería Ambiental, Universidad Nacional de Moquegua, Provincia de Mariscal Nieto, Moquegua, Peru
[c] Laboratorio de Cerámicos y Nanomateriales, Facultad de Ciencias Físicas, Universidad Nacional Mayor de San Marcos, Lima 14-0149, Peru
[d] School of Biological and Environmental Science, Liverpool John Moores University, Liverpool L3 3AF, United Kingdom

ARTICLE INFO

Article history:
Received 27 May 2021
Received in revised form
23 May 2022
Accepted 1 June 2022
Available online xxx

Keywords:
Andean river
Moquegua river
Sediments
Fourier-transform infrared spectroscopy
TG-DTG/DTA
Clustering analysis

ABSTRACT

This study presents an analysis of sediments in an Andean river impacted by both natural conditions and anthropogenic activities. Fifty samples were collected from selected sites throughout the Moquegua River drainage basin, and Tambo River headwaters at Pasto Grande, in Peru, and analysed with X-ray diffraction, energy dispersive X-ray spectroscopy, scanning electron microscopy, Fourier-transform infrared spectroscopy and thermogravimetric analysis. Si, Ca, Al, Fe, and O, common constituents of soils, were dominant, along with K, N, and P. The latter originating as primary macronutrients or chemical residuals from fertilizers used in agriculture. Higher concentrations of macronutrients and organic components were found in agricultural and urban areas, respectively. Arsenic minerals were also detected, which occur naturally, but possibly at levels augmented by anthropogenic activity. The application of cluster analysis revealed clustering between arsenic, arsenolite, and potassium but no significant geospatial correlation between sample sites in the drainage basin.

1. Introduction

In recent years, interest in understanding the geochemical dynamics of sediment loading in Andean rivers has increased, especially in arid and hyper-arid regions where mining activities are thought to augment concentrations of trace metals in rivers (Tenorio et al., 2018). However, there are few studies focusing on the use of sediments to investigate trace metal contamination in Peru. This is also true of the greater Moquegua drainage basin, which covers 3,484 km^2. The Moquegua River has its origins in the high Andes and flows to the hyper-arid pacific coast at Ilo in southern Peru, in the course of which landscape-scale copper mining and an agricultural irrigation project are being developed (see Fig. 1). The tributaries all rise in the Cordillera Occidental, at elevations above 5,000 m a.s.l. The Sajena, Torata, and Moquegua rivers meet at the city of Moquegua at 1,200 m a.s.l., below which it is variously named the Moquegua, Osmore and Ilo river as it nears the Pacific Ocean. River discharge in the Moquegua drainage basin is significantly increased with water from the Pasto Grande reservoir, in the Tambo River headwaters, which enters the Sajena river at 4,000 m a.s.l. Water from the Pasto Grande canal supplies water for both irrigation projects and domestic consumption throughout the department of Moquegua. The landscape-scale Cuajone mine (lat - 17.042616°, long - 70.707437°), in the Torata River headwaters, and the recently opened Quellaveco mine in the Asana River headwaters lie directly above the city of Moquegua (Covey, 2006; Sims, 2010).

The Cuajone mine, operated by Southern Copper, is one of the largest open cast mines in the world. It started operation in 1970 and is located in the Torata district (around 3500 m a.s.l), province

* Corresponding author.
E-mail addresses: ld301@cam.ac.uk, luisitodv@yahoo.es (L. de Los Santos Valladares).

https://doi.org/10.1016/j.ijsrc.2022.06.002
1001-6279/

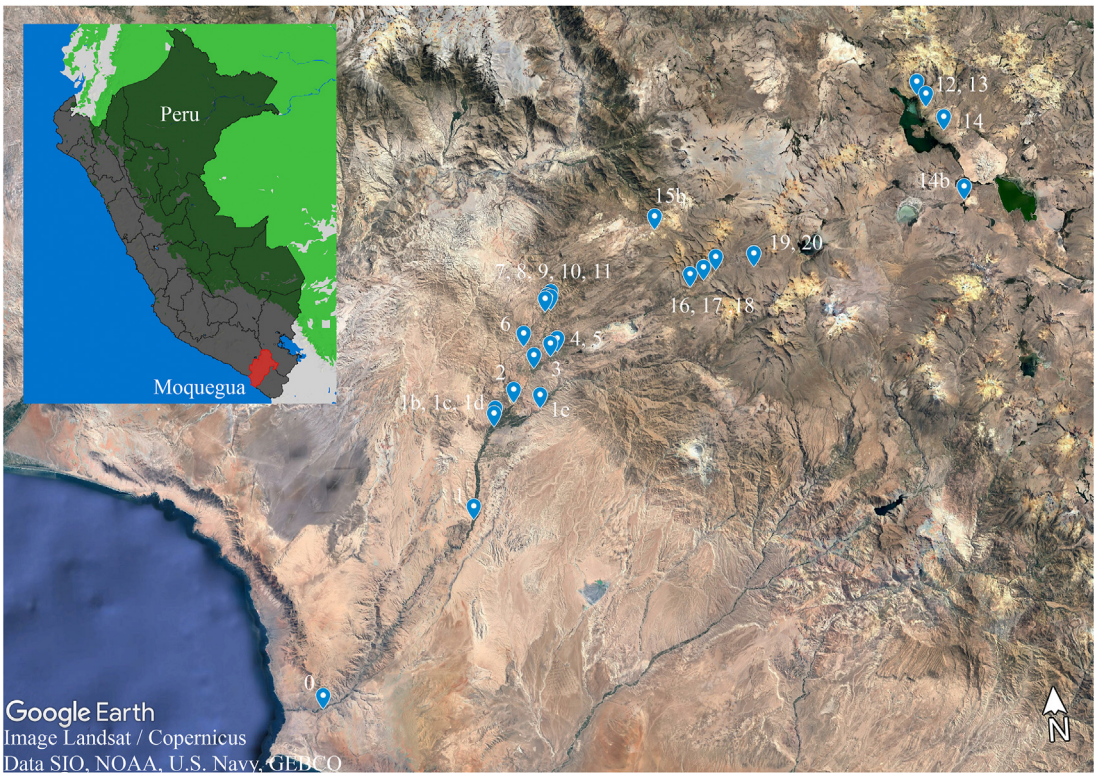

Fig. 1. Map of Moquegua Region, Peru, indicating the collection sites along the Moquegua River. Sites arranged below from the low lands at Ilo in sequence to the high Andes: Sites 0-a (Osmore River, near Ilo), 1 (El Conde), 1b (Moquegua River), 1c (Torata River), 1d (Sajena River), 1e (Moquegua River), 2 (Estuquina Bridge, Torata River), 3 (Coplay Bridge, Torata River), 4 (Canilay Bridge, Torata River), 5 (Firestation Torata River), 5-b (Below Cuajone mine, Torata River), 16 (Above Cuajone mine, upper Torata River), 17 (Above Cuajone, upper Torata River), 18 (Above Cuajone mine, upper Torata River), 19 (Titijones bog), 20 (Titijones source), 6 (Bocatoma Otora, Sajena River), 7 (Otora Bridge, Sajena River), 8 (Lower Polobaya River), 9 (Upper Polobaya River), 10 (Lower Sajena River), 11 (Upper Sajena River). Upper Sajena and Pasto Grande Canal: 15-b (Sajena River below confluence with Pasto Grande canal), Pasto Grande: 12 (Millohiro River), 13 (Antajarani River), 14 (Patara River), 14-b (Copapuju River).

of Mariscal Nieto, Moquegua Region. The Cuajone mine copper operations include extracting, grinding, and flotation of copper ore to produce copper concentrates. This is followed by the smelting of copper concentrates to produce blister copper, which is then refined to produce copper cathodes (Southern Copper Corporation, 2015). This production process produces significant quantities of molybdenum and silver. Supporting Information S1 describes the extraction process of copper in Moquegua.

The Andean Copper porphyry deposits in southern Peru and northern Chile are rich in Cu ores, mainly enargite (Cu_3AsS_4) (Cardozo & Cedillo, 1990), encrusted in sulphide rocks such as pyrite (FeS_2, iron (II) disulphide), chalcopyrite ($CuFeS_2$), chalcocite (Cu_2S), molybdenite (MoS_2, molybdenum disulphide), galena (PbS, lead (II) sulphide) and tetrahedrite ($[Cu,Fe]_{12}Sb_4S_{13}$) (see Supporting Information S1). Enargite contains around 48.4% of copper by weight and during the roasting oxidation process for the extraction of copper, most of the arsenic is volatilized and oxidized to arsenolites (As_2O_3 and As_4O_6) with only a small fraction remaining in the final slags (Dalewski, 1999; Long et al., 2012; Piret, 1999; Weisenberg et al., 1979) (see Supporting Information S1). This process may lead to acid mine drainage and elevated levels of arsenic in river water (Lengke et al., 2009).

The headwater areas are largely comprised of Puna grasslands and bofedales, grazed extensively with Alpacas, Llamas and sheep. Steep slopes from 3,000 to 1,500 m a.s.l. are extensively covered with thick scrub and grasslands. Below the Cuajone mine, extensive irrigation systems allow the cultivation of a wide range of crops, including potatoes, pulses, maize along with extensive areas of grazing land for dairy cattle. In the floodplain, below the city of Moquegua extensive areas are devoted to viticulture, avocado orchards, olive groves, and pasture land for dairy farming, with little or no small-scale subsistence production. Away from the floodplain, the desert landscape is dominated by sparse xeric scrub, grasslands and *Tillandsia* sp dominated fog vegetation. Farming in the lower Moquegua River drainage basin uses a variety of fertilizers urea ($CO(NH_2)_2$, containing 46 wt% N), potassium chloride (KCl, containing 60 wt% K_2O), mono-ammonium phosphate ($NH_4H_2PO_4$, containing 10 wt%–12 wt% N and 50 wt%–52 wt% P_2O_5), ammonium nitrate (NH_4NO_3, containing 33 wt% N and 3 wt% P_2O_5), ammonium sulphate ($(NH_4)_2SO_4$, containing 21 wt% N and 24 wt% S), potassium sulphate (K_2SO_4, containing 50 wt% K_2O and 18 wt% S), magnesium sulphate heptahidratated ($MgSO_4{\cdot}7H_2O$, also containing 16 wt% MgO and 13 wt% S), calcium triple superphosphate ($Ca(H_2PO_4)_2{\cdot}H_2O$, containing 45 wt% P_2O_5 and 15 wt% Ca) and a fertilizer called 'compound 20-20-20' (containing 20 wt% N, 20 wt% P_2O_5 and 20 wt% K_2O). Peru does not produce fertilizers and all the above compounds are imported from abroad, mainly from Russia, the USA and Canada (Fernández Massó, 2003; Sihuas, 2016).

There have been no geochemical studies of alluvial sediments in the Moquegua River drainage basin or their complex determination by a combination of both geological conditions and anthropogenic activity in the region. However, regional studies include the Chili River in Arequipa which reports no impact from the Anglo American copper mine at Cerro Verde but significant contamination from agricultural residues and sewage discharge in the lower catchment (Rotting et al., 2009). A study of the Ite Wetland, initially used as tailings dump for the Toquepala mine, operated by Southern Copper in Tacna, southern Peru reports quartz, muscovite, biotite,

Please cite this article as: de Los Santos Valladares, L et al., Physical and chemical characterization of sediments from an Andean river exposed to mining and agricultural activities: The Moquegua River, Peru, International Journal of Sediment Research, https://doi.org/10.1016/j.ijsrc.2022.06.002

plagioclase, anhydrite, gypsum, and pyrite as principal sedimentary components (Dold et al., 2006). Another study investigating colonial kilns in the Moquegua valley reported exposed gypsum ($CaSO_4 \cdot 2H_2O$) deposits in places on the desert hill sides bordering the southern part of the valley (Rice, 1994).

The traditional methods employed for sediment analysis involve wet digestion of solid samples in hot concentrated acids followed by trace element determination by inductively coupled plasma (ICP) or atomic absorption spectrometry (AAS) (Crompton, 2001). These methods are complex and time-consuming; thus, they are less suitable to analyse a massive amount of samples collected from large areas and at different seasons (Chapman & Wang, 2001). Here, we report the physical and chemical characterization of sediment samples collected from many points along the Moquegua River by more available techniques such as energy dispersive X-ray spectroscopy (EDX), X-ray diffraction (XRD) and Fourier-transform infrared spectroscopy (FTIR) which have demonstrated in other works that identifies very well feldspars, quartz, aluminium silicates as well as soil macronutrients in soils and sediments (Bustamante et al., 2012; Corzo et al., 2022). In fact, these components together with arsenolite and high concentration of organic components are found in many sites downstream of the river by these techniques. This is the first attempt to investigate the dispersion and concentration of specific trace metals in the Moquegua River drainage basin.

2. Materials and methods

2.1. Study sites

Sediment samples were collected in the Moquegua River drainage basin and at Pasto Grande during the period June 29, 2017 to July 6, 2017 at the sites indicated in Figs. 1 and 2. At each point, the sediment samples were collected directly from the bed and bank of the river. There are a total of fifty samples. Table S2.1 (Supporting Information S2) provides information about the sample sites. The sediment samples were stored in plastic containers and sent to the laboratory for *ex-situ* analysis.

2.2. Sample processing and measurements

The samples were dried at 30 °C to avoid thermal oxidation, decomposition of organic materials and phase transitions. The powder XRD studies were performed on a Bruker D8 X-ray diffractometer for phase identification in the 2θ region between 10° and 80°. This study was carried out using Cu Kα radiation at 40 kV and 40 mA with a secondary monochromator. The scanning electron microscopy (SEM)-EDX analyses were performed in a Phillips XL30 microscope equipped with an Oxford EDX detector. For the thermogravimetry analysis, the samples were not dried nor reacted with any solvent in order to keep possible organic components. The natural samples were placed on alumina (Al_2O_3) crucibles and mounted on a Linseis STA PT 1,600 to simultaneously measure thermal gravity (TG) and differential thermal analysis (DTA). The data was collected from room temperature (RT) to 1,000 °C, with a heat rate of 10 °C/min in air atmosphere and against an empty sample reference. Fourier-transform infrared spectroscopy measurements were performed in a PerkinElmer Spectrum RX-1 by averaging 32 scans at a resolution of 16 cm^{-1} in the range of 4,000–400 cm^{-1} using potassium bromide (KBr) pellets. The spectra were obtained with respect to a KBr background collected under the same measurement conditions. In order to validate the chemical composition obtained by EDX, some sediment samples were analysed by inductively coupled plasma-mass spectroscopy (ICP-MS, Agilent 7900) following a reverse aqua regia digestion in a

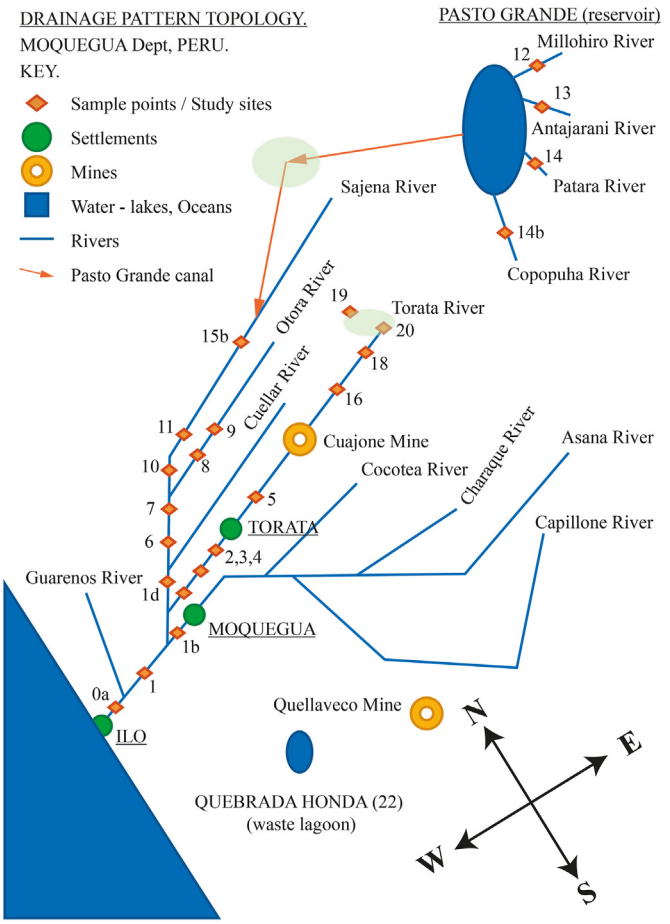

Fig. 2. Schematic representation of the Moquegua River drainage basin and sample sites. See Table S2.1 in the Supporting Information S2 for more sample site details.

CEM Mars 6 microwave digestion system. A certified reference material (BCR-277 R) was used to assess the recovery of analytes in the sediment samples which ranged from 77% to 111% for Cr, Ni, Cu, Zn and As. Unsatisfactory recovery rates were reported for Cd (182%) and Hg (2289%).

2.3. Calculation

Cluster analysis (CA) was employed to identify geochemical and geospatial patterns and associations CA is a way of producing a one-dimensional measure for the level of difference (distance) between observations, and ultimately allows the creation of groups (clusters) with small inter-cluster distances (Kazi et al., 2009; Liu et al., 2003). Here, we employ Ward's agglomerative hierarchical clustering method. In this method, all observations start in individual clusters, which are then merged in order of increasing (Euclidean) error sum of squares (McKennA, 2003; Otto, 1998). MATLAB R2021b was used to perform the statistical analysis and data clustering.

3. Results and discussion

3.1. Chemical and mineralogical composition

The sediment samples consist of sand with different shape and sizes as observed in the images of the samples provided in the Supporting Information S2. Most samples are grey in colour (typical

Please cite this article as: de Los Santos Valladares, L et al., Physical and chemical characterization of sediments from an Andean river exposed to mining and agricultural activities: The Moquegua River, Peru, International Journal of Sediment Research, https://doi.org/10.1016/j.ijsrc.2022.06.002

for silicate sands), with some white, brown, red and yellow. The colour, shape and size of the samples depends on the chemical composition and physical properties of each sample. Since there are fifty samples, we provide here the physical and chemical analysis of only one of them in detail (sample 0-a-bank). The measurements for the rest of the samples are provided in the supporting information sections. The micro-morphology of the 0-a-bank sample is shown in Fig. 3(a). Similar to all the collected samples, it consists of grains with different shapes. It was not possible to estimate the mean size of the nanograins since they stuck together, forming a cumulus. The SEM micrographs for the rest of the samples are given in Fig. S3.1 of the Supporting Information S3. No significant difference was noted between the micro-morphology of the samples. However, diatoms were observed in several samples (samples 0-a and 18; see Table S3.1 in the Supporting Information S3). These are a diverse group of micro-organisms commonly found in aquatic environments, with many species as important indicators of environmental conditions suitable for the higher forms of life (Bruland et al., 2005; de Vries & Schrader, 1981; Hutchins et al., 2002; Eppley, 1972).

The chemical composition of the samples as determined by EDX analysis was measured for selected scan areas. For example, for sample 0-a-bank, the EDX mapping was taken over the whole micrograph shown in the inset of Fig. 3(a). Similarly, for the rest of the samples, EDX analyses were taken over selected scan areas as shown in Fig. S3.1 of Supporting Information S3. The XRD analysis for the sample 0-a-bank is shown in Fig. 3(b). It provides information of the main mineralogical composition of each sample. The chemical and mineralogical composition for this and remaining samples is given in Table S3.1 (The XRD for each sample is provided in Fig. S3.2 of Supporting Information S3). We have arranged the results into groups determined by the principal compounds detected.

3.1.1. Silicates

According to the EDX results listed in Table S3.1, all the samples contain Si, Al, Ca, Na and O as the most abundant elements. This was expected since the main composition of river sands and rocks are quartz (SiO_2), alumina (Al_2O_3) and aluminium silicates ($xAl_2O_3 \cdot ySiO_2 \cdot zH_2O$, where x, y and z can be Na, Ca and K) (Gudbrandsson, 2013). In fact, according to the XRD analysis, the mineralogical composition for almost all the samples contains quartz (SiO_2) and sodium or calcium aluminium silicates.

The presence of silicon dioxide (SiO_2) is found in most of the samples. It appears in nearly all the sediment samples from the Moquegua River as quartz is the natural composition of almost all sands, while cristobalite is a high-temperature polymorph of silica (with the same chemical formula as quartz, but a distinct crystal structure) (Deer et al., 1966; Frondel, 1962; le Page & Donnay, 1976; Mason, 1972; Pluth et al., 1985). Both quartz and cristobalite are polymorphs with all the members of the quartz group, which also include coesite (formed at high pressure and temperature) (Frondel, 1962; Gibbs, 1977; Sclar et al., 1962; Smyth & Hatton, 1977), tridymite (colourless and transparent quartz) (Deer et al., 1966; Frondel, 1962; Grant, 1967; Konnert & Appleman, 1978; Wennemer & Thompson, 1984) and stishovite (hard and dense synthetic SiO_2) (Frondel, 1962; Ross et al., 1990; Sinclair & Ringwood, 1978). Cristobalite appears as white octahedra or spherulites in acidic volcanic rocks. Cristobalite is stable only above 1470 °C but can crystallize and persist as metastable at lower temperatures (Deer et al., 1966; Frondel, 1962; le Page & Donnay, 1976; Mason, 1972; Pluth et al., 1985). Note that the aspect of almost all the samples containing either quartz or cristobalite is of finely grained sand with a light grey colour (see photos of the samples in Supporting Information S2).

The main type of aluminium silicates found in the present samples was feldspar minerals: labradorite ($(Ca,Na)(Al,Si)_4O_8$), microcline ($KAlSi_3O_8$), albite ($AlNaSi_3O_8$) and anorthite ($Al_2CaSi_2O_8$). Labradorite is found in samples from the lower Moquegua River, the Sajena River and two sites in the upper Torata River, but not from Pasto Grande. Note that the high amount of Ca in the EDX analysis for these samples (more than 3 wt%for all these samples) is because this mineral is an intermediate to a calcic member of the plagioclase series containing 50 wt%–70 wt%of anorthite (Dana, 1898; Deer et al., 1966; Kempster et al., 1962; Megaw et al., 1962). The crystal system of Labradorite is triclinic and it occurs as clear, white to grey, blocky to lath shaped grains as observed in the aspect and morphology of the corresponding samples (see photos of the samples in Supporting Information S2).

Microcline is an alkali feldspar (or K-feldspar) and it forms during slow cooling of orthoclase. This feldspar mineral was found in samples 1-b bank, 4 bank and 16 bed. The small presence of Na in the mineralogical formulas of the samples (see Table S3.1) is because microcline is a potassium-rich alkali mineral and typically contains minor amounts of sodium (Rickwood, 1981). Microcline can be pale-yellow or brick-red as it is confirmed by the colour of the corresponding samples (see Supporting Information S2).

Albite is also found in large quantities in nearly all sediment samples. Albite is a plagioclase tectosilicate with less than 12 wt% anorthite ($Al_2CaSi_2O_8$, e.g. Sample 1-g bank presents 45.5 wt% of albite and 12 wt% of anorthite). Its colour is usually white as can be seen in sample 5 bed (see Supporting Information S2) where nearly 47 wt% of its composition is albite (see Table S3.1). Albite crystallizes in a triclinic pinacoidal shape and it occurs in two variants referred to as low albite and high albite (Tuttle & Bowen, 1950). Although both variants are triclinic, they differ in the volume of their unit cell, which is slightly larger for the high form. The high form can be produced from the low form by heating around 700–800 °C as it is discussed in the TG-DTA analysis below.

Andesine, $(Ca,Na)(Al,Si)_4O_8$ is found as a main component (more than 20 wt% abundance) in several samples (Sites 0-a bed, 8 bed, 11 bank, 14 bank, 14 b and 19 bank). This is a typical mineral from soils and rocks of the Andean mountains and has its origin in the andesite lava. Andesine usually occurs in intermediate igneous rocks such as diorite (around 70 wt%) and syenite (less than 10 wt %). Moreover, it characteristically occurs in metamorphic rock of granulite to amphibolite facies and commonly exhibits antiperthite texture. It also occurs as detritus grains in sediments (Steurer & Jagodzinski, 1988).

3.1.2. Soil macro and micronutrients

Primary soil macronutrients include potassium, nitrogen and phosphorus (Ajasa et al., 2004; Liu et al., 2009; Sternberg et al., 2007a). Potassium is an essential component of plant nutrition and is used as one of the main components of fertilizers in agriculture, especially in the form of potassium chloride (KCl, Sylvite) (Dmitrenko et al., 1999; Elouear et al., 2016; Kiiski et al., 2016; Prakash & Verma, 2016; Webb, 1939). EDX and XRD detected this compound primarily in farming areas in the lower drainage basin but also very widely in the headwater sample sites at Pasto Grande and the upper Torata River. These findings indicate that the alluvial soils of the lower Moquegua Valley naturally fertile, with most of it now used for agriculture. High concentration of KCl has been detected in the sites 4, 5 and 11, which are located in close proximity to farms near Torata, and plants still grew on the samples even after one week of storage in the lab (see photos of both samples in Supporting Information S2). KCl is found in nature as sylvite but it is also one of the main components of potassium chloride fertilizers (Dmitrenko et al., 1999; Elouear et al., 2016; Kiiski et al., 2016; Prakash & Verma, 2016; Webb, 1939), suggesting

Please cite this article as: de Los Santos Valladares, L et al., Physical and chemical characterization of sediments from an Andean river exposed to mining and agricultural activities: The Moquegua River, Peru, International Journal of Sediment Research, https://doi.org/10.1016/j.ijsrc.2022.06.002

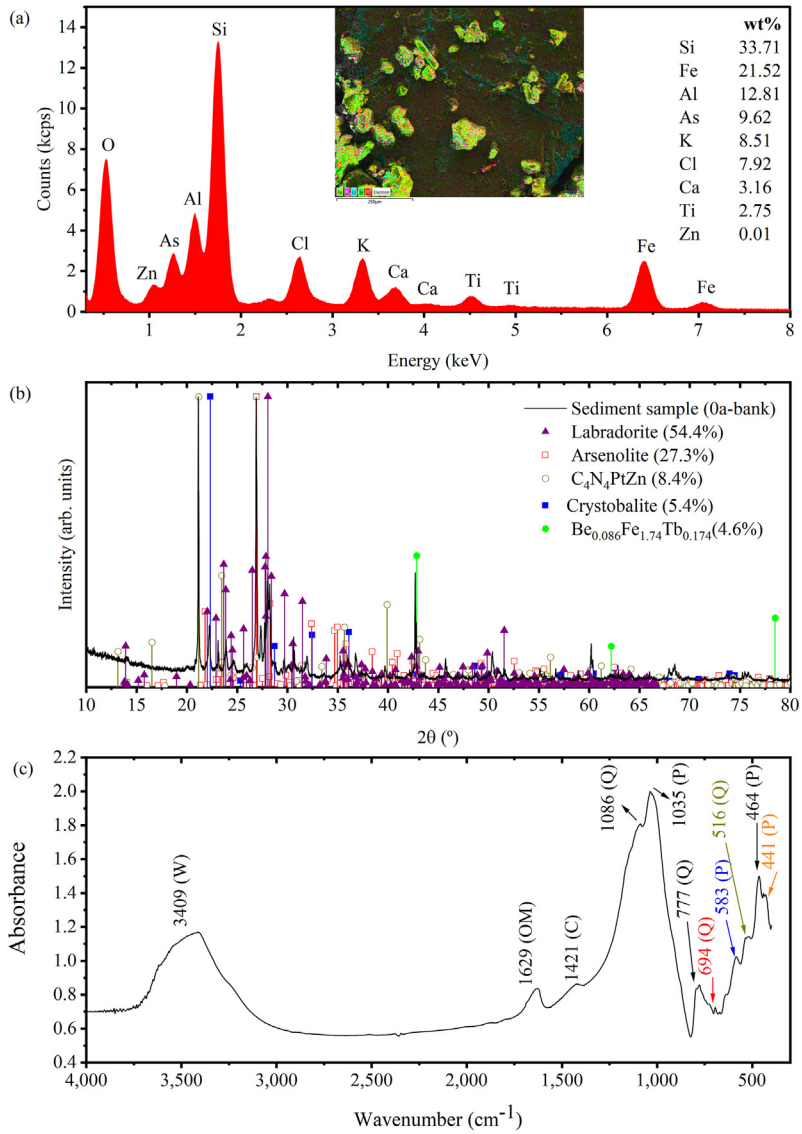

Fig. 3. Physical and chemical analysis for the sediment sample 0-a collected from the banks of the Moquegua River. (a) Chemical composition obtained by EDX and SEM micrograph (inset); (b) XRD analysis indicating the main mineralogical composition; and (c) FTIR spectrum of sample 0-a. The data for the rest of the samples are given in the Supporting Information S2, S3 and S4. (C - Carbonates, OM - Organic Matter, P - Plagioclase, Q - Quartz, W - Water.)

that environmental levels of KCl are greatly augmented by agricultural run-off.

Nitrogen is another primary macronutrient found in the samples. Nitrogen is one of the most important plant substances (it comprises 40 wt% to 50 wt% of the dry matter of protoplasm) and concentrates in chlorophyll and amino acids which are the building blocks of proteins for plants (Alvarez, 2006; Barak et al., 1997; Cerrato & Blackmer, 1990; Fischer et al., 1993; Frink et al., 1999; Jaynes et al., 2001; Kohl et al., 1971; Ledgard et al., 1999; Zhu & Chen, 2002). This element has been found together with K in sites 7 and 18. Site 7 is very close to farms and N has been found together with CO_2 and di-phosphate which led us to infer that N also comes from the rest of fertilizers such as urea, ammonium phosphate, ammonium nitrate or compound 20-20-20 used by local farmers. However, nitrates have been detected in samples from site 18, located in the Torata River headwaters, in the form of sodium nitrate ($NaNO_3$). Note that principal nitrate fertilizers contain ammonium (Alvarez, 2006; Barak et al., 1997; Cerrato & Blackmer, 1990; Fischer et al., 1993; Frink et al., 1999; Jaynes et al., 2001; Kohl et al., 1971; Ledgard et al., 1999; Zhu & Chen, 2002) which is commonly used in Peru (Fernández Massó, 2003; Sihuas, 2016). Thus, the $NaNO_3$ found in this sample most likely originates from the headwater wetlands above this site, where it is found bank rather bed samples (Browman & Gundersen, 1993; Wisniak & Garces, 2001). The presence of diatoms, detected by SEM, in the Torata headwaters may be due to higher salinities found at sample sites.

Secondary macronutrients for plants in soils include Mg, Ca and S (Ajasa et al., 2004; Liu et al., 2009; Sternberg et al., 2007b). Magnesium is as a constituent of the chlorophyll molecule, it is also involved during reaction of the enzymes during plants nutrition and it is very mobile from older to younger tissues in the plants (Härdter et al., 2005; Lixian et al., 2005; Uebel & Heinsdorf, 1997). EDX analysis has detected magnesium together with potassium at most sample sites at lower elevations in the drainage basin. Since the sites of collection of those samples are located at the North and

Please cite this article as: de Los Santos Valladares, L et al., Physical and chemical characterization of sediments from an Andean river exposed to mining and agricultural activities: The Moquegua River, Peru, International Journal of Sediment Research, https://doi.org/10.1016/j.ijsrc.2022.06.002

West of the Moquegua City, close to farms, we can assume that this area is either rich in Mg or it comes from the magnesium sulphate used by local farmers as a fertilizer. In the case of potassium, it is one of the main components of feldspar present in the whole area of study as it is discussed in more detail the FTIR analysis below. However, XRD also detects natural MgO (periclase) in the beds of sites 16 and 21 which are located to the East of the Moquegua City at two different branches of the river (see Figs. 1 and 2). It is confirmed that, in both cases, MgO derives from natural periclase rather than magnesium sulphate fertilizer since this is usually found together with iron or wüstite (FeO) (Ammann et al., 2011; Gail & Sedlmayr, 1999; Scanavino et al., 2012; Yamazaki et al., 2009), as it has also been detected by EDX in both samples (see Table S3.1).

Calcium is detected in the banks and beds of almost all the sites of study, with a high concentration (3.5 wt%–9.7 wt%) at sites lower than 2500 m a.s.l and a low concentration (0.5 wt%–3 wt%) above 2500 m a.s.l. Note that in Pasto Grande and Torata River sample sites above the Cuajone Mine natural Ca has been detected with XRD. This most likely originates from labradorite, anorthite, andesine or albite rather than calcium-phosphate fertilizer residues, since this element has been found in almost all samples, including those away from farms. The main source of this element is found in limestone in which $CaCO_3$ (calcite and aragonite) is a dominant component and an important source of nutrients for plant life (Kiiski et al., 2016). However, although $CaCO_3$ has not been detected by XRD (maybe due to its very low amount in comparison to the other components), its presence in the samples is suggested by FTIR and thermogravimetry analysis below. It seems likely that the Ca detected comes from limestones found throughout the catchment headwaters.

Sulphur has been detected at sites scattered throughout the sample site network. Sulphur is hydrophobic (not soluble in water) and it cannot be absorbed directly by plants (Ahmad et al., 2005; Nichols et al., 1990; Rangkadilok et al., 2004; Wen et al., 2001; Wooding et al., 2000). Commercial fertilizers contain this secondary macronutrient in the form of ammonium, potassium, magnesium or calcium sulphate (Ahmad et al., 2005; Nichols et al., 1990; Rangkadilok et al., 2004; Wen et al., 2001; Wooding et al., 2000). Whilst it is possible that the S found in the lower altitude Moquegua River could come from waste sulphite or sulphur dioxide as derived from chemical reactions performed at the Cuajone mine during copper extraction (see Eqs. (S1.2) – (S1.14) in Supporting Information S1), the highest concentrations of S are found at sites that are higher in altitude than the mine. For example, sample 19 bank presents around 6 wt% of sulphur and it is located well above the Cuajone mine. A similar situation occurs with sites 12, 13 and 14; they are supply rivers around the Pasto Grande reservoir and they exhibit more than 3 wt% of sulphur. We, therefore, conclude that sulphur detected comes predominantly from natural rather than from anthropogenic sources. In fact, as described in Supporting Information S1, the geology reports about Moquegua reveal that this area is rich in sulphides formed by the reaction of sulphide porphyry, rhyolite and andesite rocks.

The presence of manganese and iron has also been detected in most of the samples. Both elements constitute micronutrients for plants, but they are also likely to form alloys with other metals, including heavy metals (Tessier et al., 1979). Manganese is primarily detected at the lower elevation sites. As Mn is rarely found as a free element in nature, it is most likely detected in our study as a mineral component in our samples. This is confirmed by XRD which detects $As_7Mn_6RbO_2$ as one of the main mineral components of samples 1-e bank, 16 bed, 18 bed, 20 bank and 20 bed. In the case of iron, it has been detected by EDX in all the sites of study with a major abundance in high altitude areas (sites 12, 13, 14, 16, 18 and 20). For example, according to the EDX results, 56.87 wt% and 72.85 wt% of the elemental composition of the samples collected from the bank and bed, respectively, from site 12 is iron (see Table S3.1). Similar to the case of the sulphur discussed above, it is unlikely that these elements come from anthropogenic sources (mining or agricultural activities). It should come from iron oxides and hydrous iron contained in the rhyolite, andesite and dolerite which are the main rocks in the area of study (see Supporting Information S1). For example, siderite ($FeCO_3$) is detected by XRD in sample 3 bed. It is diagenetic and found as sandstone close to the warm water of the Moquegua River, similar to reports on hydrothermal veins in the literature (Deer et al., 1966; Effeberger et al., 1981).

In order to validate of the quantity of K, Ca and Mg macronutrients present in the soils, a comparison of the weight ratio obtained by EDX with the amounts obtained by ICP-MS is included in Table 1 for some samples. Note that, in contrast to EDX analysis, ICP-MS provides information of Mg amounts in the sample. This is because the samples are digested in aqua regia (see experimental section) and thus most of the components can be resolved by this technique. In contrast, the EDX is a more localized technique. It detects the elements localized on the surface of the sample (~1 μm deep) in which there would be lack of some elements. Nevertheless, K and Ca macronutrients are better detected by both techniques, suggesting that they are also distributed more in the surface of the samples than Mg. Remarkably, for all the samples, the amount K and Ca match well, following the same trend. For example, both techniques reveal that the amount of potassium is higher than calcium for most of the samples except for sample 20 which Ca is higher than K. Since sample 20 was collected nearby Quajone Mine, these results suggest that soil macronutrients are affected by mining activities. See Supporting Information S4 for a more extensive ICP-MS data of the samples.

3.1.3. Arsenic

Arsenic has been detected by EDX in samples 0-a bank (10 wt%) and 14 bed (4.12 wt%). Arsenic scarcely exists as a pure element because it exhibits a high affinity to form chemical bonds with other elements (Nazari et al., 2017). The As detected by EDX analysis in this work comes from natural enargite, abundant in the Andes as described in the introduction and the Supporting Information S1. This element is spread through the whole of South American by the rivers flowing from the Andean mountains (Scarpelli, 2005). In nature, As can exist in organic and inorganic compounds and it is typically the inorganic ones which are more toxic than the easy soluble organic compounds (Mandal & Suzuki, 2002). The arsenic contained in inorganic and organometallic substances in nature exists essentially in four oxidation states: −III (arsine), 0 (arsenic), +III (arsenite) and +V (arsenate) (Cherry et al., 1979; Drahota & Filippi, 2009; Nazari et al., 2017). Several studies have shown that

Table 1
Comparison of macronutrients amount obtained by EDX and ICP-MS for samples 12, 13, 14 and 20.

Sample	ICP-MS (mg/Kg)			EDX (wt%)		
	K	Ca	Mg	K	Ca	Mg
12	869.30	342.34	578.95	1.50	0.50	0.20
12 bank	2,187.33	656.38	828.83	1.86	0.34	–
12 bed	1,306.09	416.35	785.33	0.62	–	–
13 bed	3,158.98	1,079.81	3,022.38	2.23	0.55	–
14 bank	2,337.63	2,294.61	5,074.94	4.2	2.83	–
14 bed	1,138.70	859.12	2,737.02	3.82	–	–
14 b bed	1,714.46	1,237.76	1,938.95	7.36	2.93	–
20 bank	554.19	1,493.28	1,090.57	3.55	6.29	1.37
22	4,229.42	22,987.32	8,289.27	2.95	4.02	2.59

Please cite this article as: de Los Santos Valladares, L et al., Physical and chemical characterization of sediments from an Andean river exposed to mining and agricultural activities: The Moquegua River, Peru, International Journal of Sediment Research, https://doi.org/10.1016/j.ijsrc.2022.06.002

most of the naturally occurring As is contained in inorganic compounds (Cherry et al., 1979; Cullen & Reimer, 1989). Furthermore, As^{3+} concentration exceeds this of As^{5+} in the permanently oxidizing environment of surface waters and soils (Bowell et al., 1994; Cullen & Reimer, 1989; Macur et al., 2001, 2004; Sohrin et al., 1997). Both As^{3+} and As^{5+} are soluble in water; however, As^{3+} is the most toxic of the As species (Cullen & Reimer, 1989; Drahota & Filippi, 2009; Yang et al., 2013). In fact, As^{3+} is phytotoxic and hazardous to human health (ingestion is the main route of exposure, but inhalation can also have toxic effects) (Gallegos-Garcia et al., 2012; Huang & Fu, 1984). As^{3+} also threatens aquifers, streams and areas of agricultural soils (Bhumbla & Keefer, 1994; Eisler, 1994; Ettler et al., 2016; Kříbek et al., 2016; Mok, 1994; Shibayama et al., 2010). In a similar work performed by Bech et al. on soils and plants in the vicinity of a mine in Northern Peru, it is reported that arsenic is absorbed by vegetation, especially by the species *Bidens cynapiifolia* and *Eriochloa ramose* (Bech et al., 1997). A similar situation could also occur in Moquegua; since both plants are found on the banks of the Moquegua River.

On the other hand, arsenic is always found in areas where Cu mining companies operate (Ashley & Lottermoser, 1999; Azcue et al., 1995; Azcue & Nriagu, 1995; Bissen & Frimmel, 2003; Cancès et al., 2008; Davis et al., 1992; Foster et al., 1998; Hudson et al., 1997; Nesbitt & Muir, 1998; Ondrus et al., 1997; Paktunc et al., 2004; Utsunomiya et al., 2003; Williams et al., 1996) and Moquegua is not an exception. In this work, arsenic and arsenic forming alarsite ($AlAsO_4$) and arsenolite (As_2O_3) has been found in samples from many study sites in the lower drainage basin and the headwaters of the Torata River, above the Cuajone mine. Arsenolite is rare in natural environments (Drahota & Filippi, 2009). It could be formed by the oxidation of arsenic-bearing sulphides during the smelting of copper ores in the Cuajone mine (see Eqs. (S1.2), (S1.3) and (S1.6) in Supporting Information S1) or by precipitation of As from the water due to redox reactions. However, the presence of As upstream from the mine and in parallel rivers indicates that As also occurs naturally. Arsenolite contains As^{3+} (Drahota & Filippi, 2009; Nazari et al., 2017). It has an octahedral structure and can be associated with its dimorph claudelite (monoclinic) (Henke, 2009; Pertlik, 1978; Treacy & Taylor, 1981). It can be distinguished as the white dust in the collected samples in this work (see the images of the corresponding samples in the Supporting Information S2). Under normal conditions (room temperature and atmospheric pressure), arsenolite is present in the form of As_4O_6 (dimeric As_2O_3) and only above 800 °C dissociates into monomeric As_2O_3 (Šlejkovec et al., 2012) as it is discussed in more detail in the thermogravimetry analysis below.

Perera et al. (2021) conducted a parallel study on quality of water in the Moquegua River system. The study showed that Torata sites upstream of the mine are contaminated with As (14–21 μg/L), especially sites 17 and 18. Concentration of As downstream of the mine remained between 4 and 11 μg/L with the lowest concentrations just below the mine. This study suggested As contamination is most probably related to the groundwater recharge in the region. Some of the As in sediment samples are therefore precipitated from water. In that case, As is expected to present in the surface layers of the sediment particles and represented by EDX analysis rather than XRD. This is because EDX analysis may represent more of the surface layers (ca. 10 μm depth) while XRD probes more into the internal structure (ca. 100 μm depth). Study of water samples from sites 12, 13, 14 showed that water samples from site 14 contained As concentrations as high as 380 μg/L (Perera et al., 2021), where EDX analysis above also showed 4.12 wt% As in the river bed. This As is therefore possibly precipitated out of water on to sediments. Another two high-altitude sites Laguna Suches and site 14-b also contained 21–24 μg/L As yet no As was recorded in EDX measurements.

3.2. FTIR analysis

Sediment samples usually exhibit O–H stretching of bonding and non-bonding water molecules and carboxylic acids from organic compounds which can be located as a broad band around 3,430 cm^{-1} in their FTIR spectra (Findoráková et al., 2015; Oudghiri et al., 2014; Pereira et al., 2012). This band can overlap with the stretching vibration of the N–H bond from amines and amides in the range of 3,500 and 3,000 cm^{-1} (Pereira et al., 2012). Additionally, bands between 1600 and 1640 cm^{-1} in FITR spectra of sediments can be attributed to C=O and C=C stretching from carboxylates, amides and aromatic groups (Oudghiri et al., 2014).

The FTIR results are given in Table S3.1 of Supporting Information S3, while the plots are given in the Supporting Information S5. The FTIR spectrum for the sample 0-a bank is shown in Fig. 3. The FTIR measurements show that all of the samples have absorption bands in the ranges mentioned above. However, the samples with a high absorption in such bands are 0-a bank, 3 bank, 3 bed, 4 bank, 5 bank and bed, 7 bed, 12 bank and bed, and 13 bed. On the other hand, the samples with a low absorption in the aforementioned range are 0-a bed, 1-b bank, 1-d bed, 2 bank, 6 bed, 8 bed, 12, 14 b, 16 bed, 18 bank, 19 bank, 20 bank, 21 bed, and 22. These results evidence that most of the organic matter in the samples can be found in two regions; around Torata (samples 3 bank, 3 bed, 4 bank, 5 bank, 5 bed) and around Pasto Grande reservoir (samples 12 bank and bed, 13 bed). It is clear that sample 0-a bank shows large absorption bands of organic compounds due to the presence of diatoms. It is also evident that samples coming from Pasto Grande have a higher absorption in bands between 3,500 and 3,000 cm^{-1}, while those taken around Torata show a higher absorption around 3,400 cm^{-1}. This difference may be an indication of the differences in the chemical composition of the organic matter between the samples.

Minerals have few but more intense IR absorption bands than most organic compounds and sediments are a composite of many minerals (Ramasamy et al., 2009). However, the assignation and identification of inorganic compounds is more complex than for the organic counterpart due to the wide absorption bands and irregular profiles (Reig, 2002). The structure of the compound plays a crucial role in the appearance of the spectra, as compounds with the same chemical composition but different structure will show different spectral profiles (Reig, 2002). Related to the region below 1700 cm^{-1}, numerous minerals exhibit their IR vibration and the assignation of bands in composite samples is not a straightforward task (Kovac et al., 2005). Therefore, the analysis of the spectrum and the assignation of the minerals to the bands was performed using the available literature (Bertaux et al., 1998; Carnin et al., 2012; Daqing, 1999; Findoráková et al., 2015; Grzechnik, 1999; Kovac et al., 2005; Matteson & Herron, 1993; Oudghiri et al., 2014; Pereira et al., 2012; Tang et al., 2015; Tironi et al., 2012) and the information obtained by XRD. This leads to a non-exhaustive identification of peaks shown in Table S3.1 of Supporting Information S3.

The feldspar group of minerals are a common constituent of river sediments (Ramasamy et al., 2009). The characteristic bands are visible in different ranges according to their chemical composition and structure, type of stretching or bending modes. In the ranges of 1,163–1,093 cm^{-1} and 1,039–931 cm^{-1}, the absorption is mainly assigned to the Si–O and Si(Al)–O stretch, respectively. The bands between 788 and 757 cm^{-1} can be attributed to Si–Si stretch, while the Si–(Al)–Si stretch is responsible for bands between 740

Please cite this article as: de Los Santos Valladares, L et al., Physical and chemical characterization of sediments from an Andean river exposed to mining and agricultural activities: The Moquegua River, Peru, International Journal of Sediment Research, https://doi.org/10.1016/j.ijsrc.2022.06.002

and 669 cm^{-1}. The bands between 650 and 580 cm^{-1} can be ascribed to the O–Si(Al)–O bend. The coupling between the O–Si–O and M–O stretches corresponds to bands between 533 and 464 cm^{-1}, while the Si–O–Si deformation shows a peak around 428 cm^{-1} (Matteson & Herron, 1993). Plagioclase and K-feldspar exhibit the same vibrations with only a slight difference in the total range of each band, i.e., the presence of two or more feldspars would produce a large overlap in the absorption bands. Therefore, the abundance of one type in the sample would obstruct the detection of the other one by FTIR. However, the identification of specific bands made the determination of each type of feldspar possible.

According to the results from Table S3.1 in Supporting Information S3, plagioclase feldspar is present in all of the samples taken and it represents one of the major constituents in most of the samples. Nonetheless, samples 2 bank, 3 bed, 5 bank, 5 bed, 9 bank, 14 b, 16 bank, 16 bed, and 22 do not exhibit large absorption bands for plagioclase feldspar, while this is different for the rest of the samples. However, the overlap of absorption bands made it difficult to identify the type of plagioclase feldspar, e.g., labradorite, albite, etc. Therefore, the different types of feldspar were identified by XRD analysis above.

K-feldspars are also present as microcline and oligoclase feldspars. Table S3.1 indicates that microclase is present in only few samples while oligoclase is present in almost half of the samples. This may be an indication for a larger amount of K-feldspars in the region surrounding Torata. However, the plagioclase feldspars and silicon dioxide are still the predominant components in the river sediments.

Silicon dioxide in the shape of cristobalite and quartz is also present in several samples and several of its bands overlap with those from feldspars. The Si–O asymmetrical bending vibrations appear in the ranges of 461–464 cm^{-1} and 509–514 cm^{-1}, while the Si–O symmetrical bending vibration is in the range of 690–695 cm^{-1}. The Si–O symmetrical stretching vibrations can be ascribed to bands in the range of 776–780 cm^{-1} and 795–800 cm^{-1}, while the 1,080–1,085 cm^{-1} and 1,169–1,174 cm^{-1} absorption region arises from Si–O asymmetrical stretching vibrations due to Al for Si substitution (Ramasamy et al., 2009). Cristobalite and quartz exhibit quite similar absorption bands to feldspar, with slightly different ranges and considerable overlaps. However, the Si–O bending vibration arises at 470 cm^{-1} and 515 cm^{-1} for quartz and at 491 cm^{-1} as a singlet for cristobalite (Daqing, 1999). Additionally, the Si–O–Si symmetrical stretching vibration appears at 780 cm^{-1} and 799 cm^{-1} as a doublet for quartz, which is its most characteristic vibration, and at 796 cm^{-1} for cristobalite (Tang et al., 2015). However, silicon dioxide is not detected by FTIR in only few samples. The rest of the samples show clear absorption bands belonging to SiO_2, in most of the cases due to the presence of quartz. On the other hand, absorption bands coming from cristobalite are found in a few mid and upper drainage basin sample sites. These results not only indicate the abundance of quartz over cristobalite, but also the low content of SiO_2 upstream towards the Sajena river and upstream towards the Cuajone mine.

As mentioned in the previous section, other minerals commonly found in sediments are arsenolite, claudite, $CaCO_3$ (calcite or aragonite) and other carbonates (such as $MgCO_3$, $PbCO_3$, etc.) for which the absorption bands can overlap with those from silicon dioxide and feldspars. In fact, the FTIR analysis do not show any peak from arsenic minerals or claudelite although the XRD results indicate a high content of them in samples from sites from the Torata River below the Cuajone mine. In the case of arsenolite, it has three important bands of absorption at around 1,425, 876, 716 cm^{-1} (Grzechnik, 1999). However, the overlap of bands with other compounds such as quartz and cristobalite may impair the detection of arsenolite by FTIR and therefore it is not mentioned in the respective column of Table S3.1. In the case of $CaCO_3$, FTIR usually presents absorption bands around 1,432, 876 and 713 cm^{-1}, while other carbonates can have additional bands at 798, 779, 729 and 690 cm^{-1} (Carnin et al., 2012; Findoráková et al., 2015; Kovac et al., 2005). In this work, only few samples exhibit a traceable content of carbonates: 0-a bank, 3 bank, 4 bank, 4 bed, 6 bed, 12 bank, 14 bed, and 21 bank. This result resembles that obtained for organic matter; most of the carbonates are obtained in two regions: around Torata and at high altitudes near the *Pasto Grande reservoir*.

The FTIR analysis also determined the presence of other compounds such as kaolinite ($Al_2Si_2O_5(OH)_4$), anorthite and siderite. Siderite is detected in sample 3-b at around 1419 cm^{-1} in good agreement with the XRD results. Anorthite is identified in samples 2 bank and 16 bank. Finally, kaolinite is a clay mineral that is present in nearly all sample sites. In most of these cases only the characteristic bands at around 3694 cm^{-1} and 3619 cm^{-1} arise in the FTIR spectrum (Bertaux et al., 1998; Tironi et al., 2012). These results suggest a low quantity of kaolinite in most of the samples, although a more exhaustive analysis is necessary to confirm this.

A selected representative FTIR spectrum of sediment sample 0-a bank is shown in Fig. 3(c) for the range 4,000 cm^{-1} to 450 cm^{-1}. The observed wavenumbers for all the samples are reported in Table S3.1. The figure demonstrates that sample 0-a may contain a considerable quantity of water (H_2O) and organic matter (OM) due to intense bands at around 3,430 cm^{-1} and 1,629 cm^{-1}. The large presence of plagioclase feldspar (P) produces an intense band around 1,035 cm^{-1} and less intense bands at 583, 464, 429 cm^{-1}. Bands at 1,086, 777, 694, 516 cm^{-1} arise due to the presence of quartz. Moreover, a slight content of carbonates produces a peak at 1421 cm^{-1}. The results partially agree with those found by the XRD analysis. Furthermore, FTIR analysis determines the presence of a plagioclase feldspar, with labradorite as a probable candidate, as determined by XRD. However, FTIR results indicate the presence of quartz instead of cristobalite and also detect some content of carbonates which is not detected by the XRD.

3.3. Thermogravimetric analysis

Thermogravimetric measurements were performed in all the samples in order to check the chemical weathering, phase transition and carbon release for all the samples. Fig. 4(a) and (b) show the TG-DTA measurements for sample 0-a-bank. The TG-DTA measurements for the rest of the samples are given in the Supporting Information S6. The TG signal for the 0-a-bank sample reveals the first weight loss of approx. 7.23% at 85.6 °C due to evaporation of water. This high value confirms the FTIR results above which revealed that this sample contains a high amount of water. It also presents two more small weight losses (less than 1%) in the temperature interval between 120 and 400 °C and at 465 °C. The DTA loop shows four main endothermic/exothermic regions due to internal reactions taking place when increasing the temperature.

Table S7.1 of Supporting Information S7 lists the weight losses (in % of total sample weight) and the temperatures at which these occurred, obtained by TG-DTG, while Table S7.2 list the endothermic/exothermic temperatures at which reactions during heating the samples occur (obtained from the DTA loops after removing the background, see Supporting Information S7). In Table S7.1, the temperatures were estimated from the peaks of the DTG loops since they represent the maximum inflexion of the TG loops. Water evaporates at different temperatures below 100 °C for all samples. The full width at the half maximum (FWHM) of these peaks are also listed. From the table, the lowest water evaporation temperatures and narrowest FWHM values are found for the sediments collected

Please cite this article as: de Los Santos Valladares, L et al., Physical and chemical characterization of sediments from an Andean river exposed to mining and agricultural activities: The Moquegua River, Peru, International Journal of Sediment Research, https://doi.org/10.1016/j.ijsrc.2022.06.002

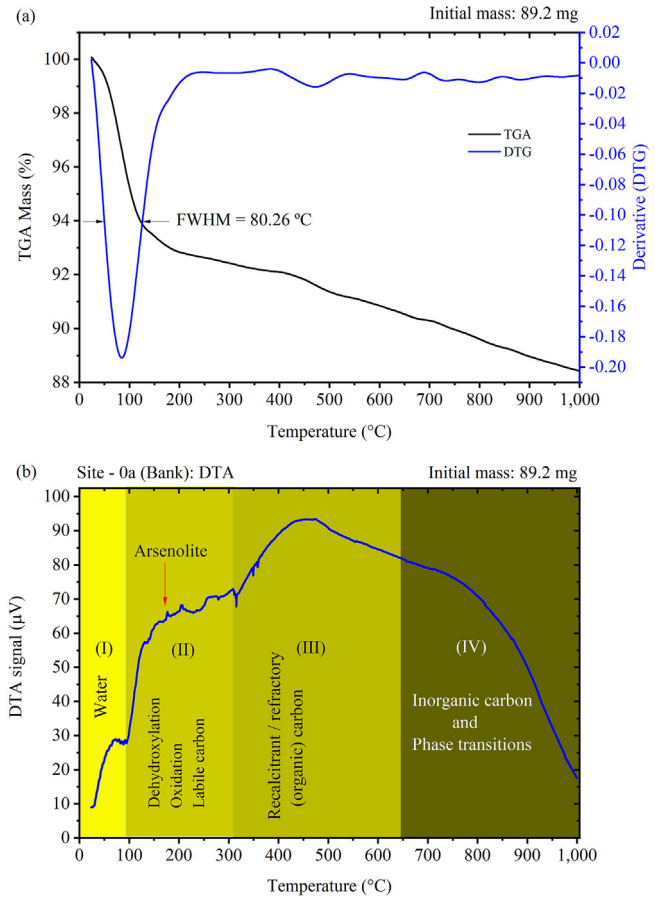

Fig. 4. TG-DTG (a) and DTA (b) measurements of a sediment sample (sample 0-a-bank) collected from the Moquegua River, Peru. The TG-DTA data for the rest of the samples are given in the Supporting Information S6.

from the banks of sites 5 (T = 58.7 °C, FWHM = 31.83 °C) and 11 (T = 40.2 °C, FWHM = 29.64 °C), meaning that water escapes easily from both samples as the temperature increases. In contrast, the highest values found for the samples collected from sites 12 bank (T = 92.8 °C, FWHM = 117 °C) and 13 bed (T = 87.2 °C, FWHM = 101.03 °C) indicate that those samples tend to retain water until higher temperatures than the rest of samples. The corresponding values for the sample 0-a bank are T = 85.7 °C, FWHM = 80.26 °C and W_{loss} = 7.28%, which fall inside the range of values for the rest of the samples (see Table S7.1). Furthermore, after the release of water, there are some other minor weight losses which might be due to volatile organic matter (Gaál et al., 1994; Schnitzer et al., 1964), as we discuss below.

The information provided in Table S7.1 will be useful for a future study that we will perform about the chemical weathering properties and erosion of soils in the Andean mountains in Moquegua since the evaporation temperature of water, the FWHM and the weight loss (W_{loss}) values provide semi-quantitative information about the wettability and hygroscopic properties of the sediment samples (Gaál et al., 1994; Schnitzer et al., 1964). Hygroscopic properties of sediments usually depend on many factors such as salt composition, porosity, granularity, organic composition, etc. For example, it has been reported that some salts and hydroxide components in sediments, such as calcium chloride ($CaCl_2$), sodium hydroxide (NaOH), potassium hydroxide (KOH), potassium chloride (KCl), zinc chloride ($ZnCl_2$), etc. (Schnitzer et al., 1964), attract water molecules making the sample more hygroscopic. Note that, according to Table S7.1, the highest weight losses are observed for samples 5 bank (12.33%) and 20 bed (54.89%) revealing that both samples contained the highest amount of water than the rest of samples. However, no salt has been detected in these samples (see Table S3.1) but some K which might come from KCl. If that is the case, KCl should be the responsible for retaining water in these samples, which is abruptly released when increasing the temperature. Nevertheless, K exists in many other samples which do not show the same behaviour. Similarly, it has been reported that sediments containing iron quickly dehydrates when increasing the temperature to form iron oxides (Rowell, 1994). If that is the case, water should dehydrate more easily in those samples containing high concentration of iron. This suggestion matches well with the quick weight loss noted in Table S7.1 and the TG loops for samples 1-d bank, 8 bed, 10 bank, 14 bank, 14-b bed, 20 bed, and 21 bed. However, this element is present at high concentration in most of the samples, especially in samples 12, and none of them follow this assumption. Therefore, the hygroscopic properties of the sediments should be also related by other physical or chemical properties of the samples (e.g., porosity, organic components, etc.).

Note that sand tends to store more water than rocks, thus it is reasonable to believe that those samples with fine grains would keep more water than those with large grains. Further studies are needed about the grain size and polydispersion of the samples in order to draw a better relationship between granularity and hygroscopic properties in these sediments. On the other hand, Gaál et al. (1994) proposed that water also binds on the surface of the sediment particles by adsorption and those grains containing more organic material bind more water due to colloid chemical forces (Gaál et al., 1994). This was agreed by Oudghiri et al. (2015) who also proposed that DTG loops of sediments containing high concentration of organic components show a big peak at around 200–300 °C and those containing a high concentration of inorganic carbon show a big peak at around 600–700 °C (Oudghiri et al., 2014, 2015; Oudghiri Idrissi Youssefi et al., 2015). Note that the DTG loops for the samples 1-f, 8 bed, 10 bank, 14 bank, 14-b bed, 20 bed, and 21 bed reveal tiny or no peaks between 200 and 300 °C and, following this assumption, the amount of organic components in these samples are insignificant to retain water molecules when increasing the temperature. This result agrees well with that obtained by FTIR above which suggests that these samples (mainly collected from the highlands in Moquegua) contain low amount of organic carbons than those collected around Torata.

Fig. 4(b) shows the DTA loop for the sample 0-a bank. The DTA loops for the rest of the samples are given in the Supporting Information S6. The DTA curve for this sample is quite similar to the others but with some differences in the intensity and positions of the endothermic and exothermic peaks (see Supporting Information S7). For a better discussion of the thermal processes in this and the rest of the samples, we divided it into four zones:

Zone I: The first endothermic peak shown in the DTA loops near 100 °C for most of the samples is caused by the contact of hot water with the chemical components of the samples just before evaporation (Rowland, 1952).

Zone II: The DTA loops between 100 and 300 °C show many small endothermal and exothermal peaks which come from multiple reactions. Among them: (i) dehydroxylation, released hydrogen reacts with oxygen from the air to form water which in turns reacts with the surface of the sample (Brindley et al., 1967; Palacios et al., 2012); (ii) oxidation of organic and inorganic components which results in the release and burn of a lot of low-molecular-weight hydrocarbons (Oudghiri et al., 2015). Gaál et al. (1994) reported that during this stage, gaseous hydrocarbons (CH_4, $CH_2{=}CH_2$, etc.) and tar are produced but only in trace amounts (Gaál et al., 1994); (iii) decarboxylation, carbon from easy-volatile organic matter (highly-reactive labile carbon) is released

Please cite this article as: de Los Santos Valladares, L et al., Physical and chemical characterization of sediments from an Andean river exposed to mining and agricultural activities: The Moquegua River, Peru, International Journal of Sediment Research, https://doi.org/10.1016/j.ijsrc.2022.06.002

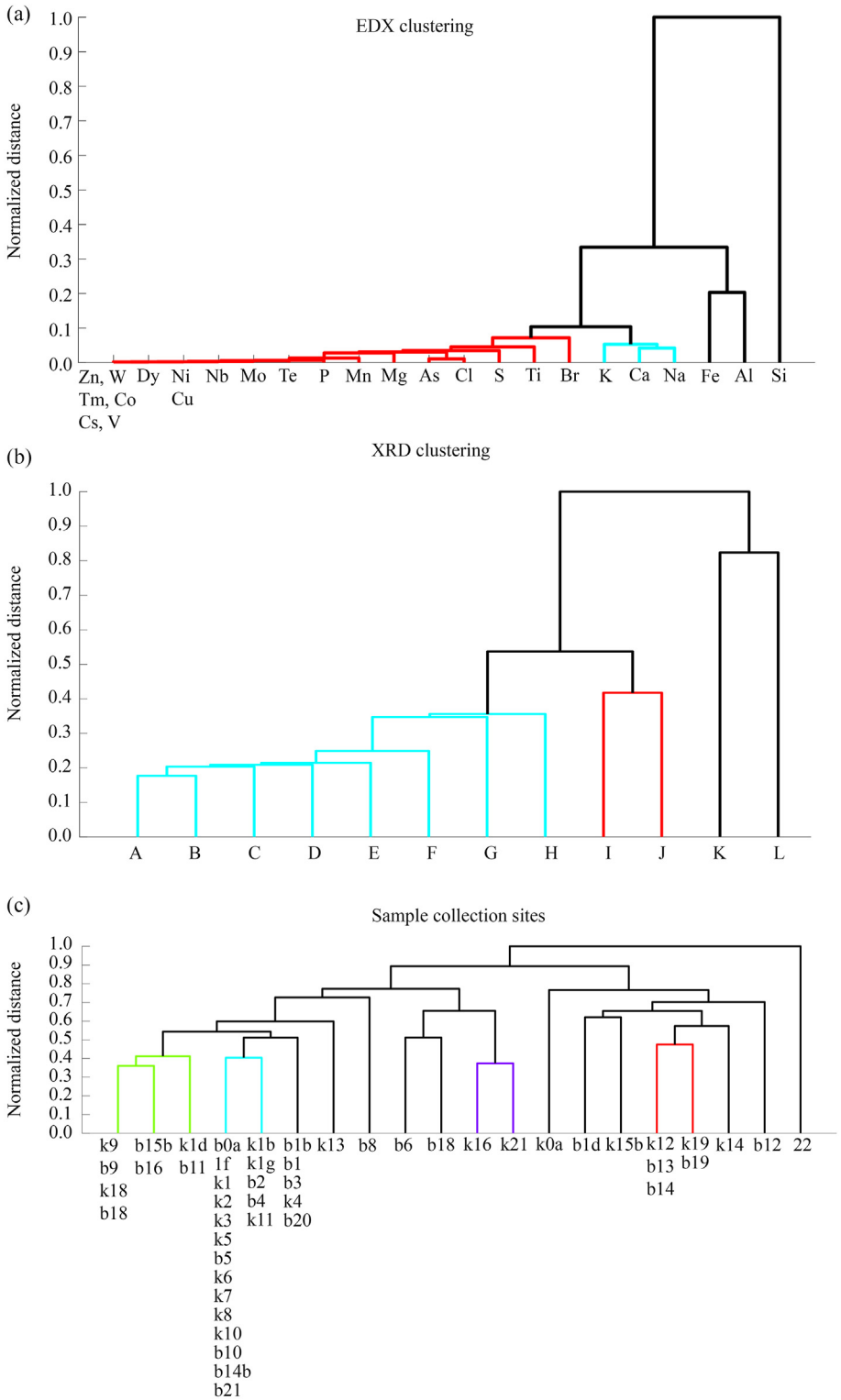

Fig. 5. (a) Hierarchical clustering dendrogram of elements found in the sediment samples collected along the Moquegua River, Peru. The %wt of these elements were found using EDX spectroscopy. The CCC is 0.99. (b) Hierarchical clustering dendrogram of crystals analysed through XRD for sediment samples collected along the Moquegua River, Peru. The CCC is 0.99. The minerals are labelled the *x* axis A through L. These groups respectively refer to: A- $Al_{1.45}Na_{1.45}Si_{0.55}O_4$, Labradorite, Albite, Labradorite, Cuprite, Albite, Tribariumaluminiumfluoride, Albite, Siderite, Albite, Microcline, Ironoxidehydroxide, Goethite, $C_4N_5S_3$, Sylvite, Sodiumnitrite, Aluminium-orthophosphate, Copper (II), Iron (III), Diphosphate, Nitrogen, Carbon dioxide, $Ca_2Fe_{0.45}Mg_{0.55}Si_2O_7$, Cristobalite, As_2TiO_2, Andesine, Sylvite, Calcium, Silver-sulphate, α-Argentite, Sodium-calcium-aluminosilicate, Anorthite-sodian, Cossaite, Hauyne, Sodium Azide, Potassium-aluminiu-morthosilicate, Anorthite; B- Henrymeyerite, $Cu_2Fe_2Ge_4O_{13}$; C- Katayamalite; D- Leucite, Labradorite; E- Labradorite; F- Alarsite, Labradorite; G- Iron; H- Microcline; I- Cristobalite; J- Andesine; K- Labradorite; and L- Iron-vanadium-molybdenum-oxide. (c) Hierarchical clustering dendrogram of sample sites. Clustering is based on XRD analysis. The CCC is 0.62, "b" stands for bed and "k" stands for bank, meaning that the samples were collected from the bed and banks of the river, accordingly.

Please cite this article as: de Los Santos Valladares, L et al., Physical and chemical characterization of sediments from an Andean river exposed to mining and agricultural activities: The Moquegua River, Peru, International Journal of Sediment Research, https://doi.org/10.1016/j.ijsrc.2022.06.002

reacting with oxygen from the air to form CO_2 (Capel et al., 2006; Lopez-Capel et al., 2006; Plante et al., 2005; Wang et al., 2011); and (iv) some phase transitions of the components (Rowland, 1952). For example, the DTA curve for sample 0-a bank shown in the figure presents a small endothermic peak around 180 °C which may come from the transition from cubic (alpha) to monoclinic (beta) of the arsenolite contained in this sample. Similar situation occurs in the case of samples 1-b bed, 1-e bank, 2 bank, 3 bank and bed, 4 bank, 5 bank and bed, 6 bed, and 21 bank (see Table S7.2 and Supporting Information S6). Also, the endothermic peak at around 315 °C might reflect one the oxidation transitions of iron (Dumitru, 1976).

Burning the sample at temperatures up to 300 °C primarily results in the release of internal water from the samples and decomposition of easily-volatile organic components generating gaseous products, such as CO and CO_2, aliphatic hydrocarbons, aromatic ethers and other molecular intermediate fragments (Oudghiri et al., 2015) which are further decomposed at higher temperatures.

Zone III: Above 300 °C, combustion of recalcitrant organic matter and refractory carbon occurs (Gaál et al., 1994; Lopez-Capel et al., 2006; Mecozzi et al., 2008; Sohi et al., 2001). The release of CO_2 increases with temperature (Oudghiri et al., 2015). This carbon dioxide should react with the hot surrounding air to form a weak acid leading a broad exothermal peak in the DTA loops between 350 and 650 °C and making the samples to loss some mass, as noted in Table S6.1.

Zone IV: The DTA loops of the samples show broad shoulders above 650 °C which is caused by either i) the release of inorganic carbon (mainly from carbonates of Ca^{2+}, Mg^{2+}, Pb^{2+}, etc.) (Rodríguez-Barroso et al., 2006); and/or ii) phase transition of some mineral components (Lopez-Capel et al., 2006; Oudghiri et al., 2014; Oudghiri Idrissi Youssefi et al., 2015; Wang et al., 2011). If the effect is caused by the release of inorganic carbon, it is accompanied with a relative high weight loss in the TG-DTG loops. For example, note that the TG-DTG loop for the sample collected from site 3 bank (see Supporting Information S6) shows high values of weight loss (3.19%) at 746 °C, which is caused by volatilization of calcium carbonate ($CCaO_3 \rightarrow CaO + CO_2$), as it was also detected by the FTIR analysis above. On the other hand, mineral phase transitions are better detected by the formation of the sharp exothermic peaks in the DTA plots. For example, the sharp exothermal peak on the DTA loop for the sample collected from site 7 bed detected around 780 °C (see Supporting Information S6) should be caused by the transition from low to high albite (Tuttle & Bowen, 1950), while those exothermal peaks detected above 800 °C for the samples collected from sites 4 bank and 5 bed should be caused by the disassociation of As_4O_6 (dimeric As_2O_3) into monomeric As_2O_3 (Šlejkovec et al., 2012).

3.4. Statistics analysis

As mentioned in Section 2.3 above, in this work we use CA to produce dendrograms showing the dissimilarity distance between the sample sites with respect to a reduced set of parameters of interest. The faithfulness of the dendrogram (how well it preserves the pairwise distance between of the original data) is given by the cophenetic correlation coefficient (CCC) – the closer to 1, the better the fit with the original, unclustered, data (Sokal & Rohlf, 1962). Fig. 5(a) and (b) show the cluster dendrograms for elements analysed with EDX spectroscopy and the crystals found with XRD respectively. The element clustering as a result of EDX analysis provides a good estimate of the abundance of elements across all study sites. The %wt of all elements at each site is shown in Supporting Information S3. XRD clustering also reveals that crystals cluster in order of abundance across all sample sites. Fig. 5(c) shows that there is no clear clustering with respect to the spatial location (see Figs. 1 and 2) of the study sites. A CCC of 0.62 is indicative that the clustering is very poor and that correlations between study sites are weak. Fig. 5(c) shows little evidence of clustering with respect to the spatial location. A number of the lower altitude sites cluster with the upper ones. The cluster analysis cannot provide significant support that the levels of {As, As2O3} and {K, S, SiO2} are affected by mining or agricultural activities. Therefore, further sampling is needed for a more reliable estimation.

4. Conclusions

This study is the first attempt to identify natural and anthropogenic determinants of alluvial sediment geochemistry in the Moquegua River and Pasto Grande, in the Tambo River headwaters, Peru. Sediment samples, collected from a comprehensive sample site network were analysed using robust physical and chemical techniques. Results indicate that, in addition to the natural silicate components Si, Ca, Al, Fe and O the N, K and P residues are most likely derived from agricultural runoff in the lower Moquegua Valley. Soils macro- and micronutrients found upstream come from natural rock sedimentation, whereas downstream they are anthropogenically increased mainly due to abuse of fertilizers by local farmers. Furthermore, many samples contain As, which could come from natural minerals or by precipitation of As in water during redox reactions. The FTIR analysis confirms that plagioclase feldspars and quartz are the main components of the river sediments and that most of the organic concentrates around Torata. The thermogravimetric analysis reveals that water contained in the samples evaporates at different temperatures below 100 °C, depending on the amount of organic material they contain. Phase transitions of some components such as that one from cubic (alpha) to monoclinic (beta) of arsenolite at around 180 °C and that from low to high albite are also detected. It was not possible to see clear clustering with respect to the spatial location of the sample sites. In employing a variety of physical and chemical methods and applying a range of robust statistical techniques we have contributed to investigations into the origins, dispersion and concentration of soluble residues in drainage basins in the region.

Declaration of competing interest

The authors declare that they have no known competing financial interests or personal relationships that could have appeared to influence the work reported in this paper.

Acknowledgements

This work was funded by a Pilot Collaboration project (Grant No. RG85120) between the University of Cambridge (UK) and the Universidad Nacional de Moquegua (Peru). The authors thank A. Quispe and W. Zeballos for administrative support during collection of samples. Part of the work has been supported by the Incorporación de Investigadores Program of the CONCYTEC – FONDECYT. UNMSM (Contrat No. 12–2019 – FONDECYT – BM – INC.INV.), Peru.

Appendix A. Supplementary data

Supplementary data to this article can be found online at https://doi.org/10.1016/j.ijsrc.2022.06.002.

References

Ahmad, A., Khan, I., Anjum, N. A. M., Diva, I., Abdin, M. Z., & Iqbal, M. (2005). Effect of timing of sulfur fertilizer application on growth and yield of rapeseed. *Journal of Plant Nutrition, 28*(6), 1049–1059, https://doi.org/10.1081/PLN-200058905

Ajasa, A. M. O., Bello, M. O., Ibrahim, A. O., Ogunwande, I. A., & Olawore, N. O. (2004). Heavy trace metals and macronutrients status in herbal plants of Nigeria. *Food Chemistry, 85*(1), 67–71, https://doi.org/10.1016/j.foodchem.2003.06.004

Alvarez, R. (2006). A review of nitrogen fertilizer and conservation tillage effects on soil organic carbon storage. *Soil Use and Management, 21*(1), 38–52, https://doi.org/10.1111/j.1475-2743.2005.tb00105.x

Ammann, M. W., Brodholt, J. P., & Dobson, D. P. (2011). Ferrous iron diffusion in ferro-periclase across the spin transition. *Earth and Planetary Science Letters, 302*(3–4), 393–402, https://doi.org/10.1016/j.epsl.2010.12.031

Ashley, P. M., & Lottermoser, B. G. (1999). Arsenic contamination at the mole river mine, northern New South Wales. *Australian Journal of Earth Sciences, 46*(6), 861–874.

Azcue, J. M., Mudroch, A., Rosa, F., Hall, G. E. M., Jackson, T. A., & Reynoldson, T. (1995). Trace elements in water, sediments, porewater, and biota polluted by tailings from an abandoned gold mine in British Columbia, Canada. *Journal of Geochemical Exploration, 52*(1–2), 25–34.

Azcue, J. M., & Nriagu, J. O. (1995). Impact of abandoned mine tailings on the arsenic concentrations in Moira Lake, Ontario. *Journal of Geochemical Exploration, 52*(1–2), 81–89.

Barak, P., Jobe, B. O., Krueger, A. R., Peterson, L. A., & Laird, D. A. (1997). Effects of long-term soil acidification due to nitrogen fertilizer inputs in Wisconsin. *Plant and Soil, 197*(1), 61–69, https://doi.org/10.1023/A:1004297607070

Bech, J., Poschenrieder, C., Llugany, M., Barceló, J., Tume, P., Tobias, F. J., Barranzuela, J. L., & Vásquez, E. R. (1997). Arsenic and heavy metal contamination of soil and vegetation around a copper mine in Northern Peru. *Science of the Total Environment, 203*(1), 83–91.

Bertaux, J., Froehlich, F., & Ildefonse, P. (1998). Multicomponent analysis of FTIR spectra; quantification of amorphous and crystallized mineral phases in synthetic and natural sediments. *Journal of Sedimentary Research, 68*(3), 440–447, https://doi.org/10.2110/jsr.68.440

Bhumbla, D. K., & Keefer, R. F. (1994). *Arsenic mobilization and bioavailability in soils*.

Bissen, M., & Frimmel, F. H. (2003). Arsenic—a review. Part II: Oxidation of arsenic and its removal in water treatment. *Acta Hydrochimica et Hydrobiologica, 31*(2), 97–107.

Bowell, R. J., Morley, N. H., & Din, V. K. (1994). Arsenic speciation in soil porewaters from the Ashanti Mine, Ghana. *Applied Geochemistry, 9*(1), 15–22.

Brindley, G. W., Sharp, J. H., Patterson, J. H., & Narahari, B. N. (1967). Kinetics and mechanism of dehydroxylation processes, I. Temperature and vapor pressure dependence of dehydroxylation of kaolinite. *American Mineralogist, 52*(1–2), 201–211.

Browman, D. L., & Gundersen, J. N. (1993). Altiplano comestible earths: Prehistoric and historic geophagy of Highland Peru and Bolivia. *Geoarchaeology, 8*(5), 413–425, https://doi.org/10.1002/gea.3340080506

Bruland, K. W., Rue, E. L., Smith, G. J., & DiTullio, G. R. (2005). Iron, macronutrients and diatom blooms in the Peru upwelling regime: brown and blue waters of Peru. *Marine Chemistry, 93*(2–4), 81–103, https://doi.org/10.1016/j.marchem.2004.06.011

Bustamante, A., Fabián, J., Santos, L. D. L., Barnes, C. H. W., & Majima, Y. (2012). Mössbauer study of contaminated soils by industrial activity in Paramonga city, Region Lima Provinces, Peru. *Hyperfine Interactions, 211*(1–3), 147–152, https://doi.org/10.1007/s10751-012-0591-x

Cancès, B., Juillot, F., Morin, G., Laperche, V., Polya, D., Vaughan, D. J., Hazemann, J.-L., Proux, O., Brown, G. E., Jr., & Calas, G. (2008). Changes in arsenic speciation through a contaminated soil profile: A xas based study. *Science of the Total Environment, 397*(1–3), 178–189.

Capel, E. L., de la Rosa Arranz, J. M., González-Vila, F. J., González-Perez, J. A., & Manning, D. A. C. (2006). Elucidation of different forms of organic carbon in marine sediments from the Atlantic coast of Spain using thermal analysis coupled to isotope ratio and quadrupole mass spectrometry. *Organic Geochemistry, 37*(12), 1983–1994, https://doi.org/10.1016/j.orggeochem.2006.07.025

Cardozo, M., & Cedillo, E. (1990). Geologic-metallogenetic evolution of the Peruvian Andes. In *Stratabound ore deposits in the Andes* (pp. 37–60). Springer Berlin Heidelberg, https://doi.org/10.1007/978-3-642-88282-1_2

Carnin, R. L. P., Folgueras, M. V., Luvizão, R. R., Correia, S. L., da Cunha, C. J., & Dungan, R. S. (2012). Use of an integrated approach to characterize the physicochemical properties of foundry green sands. *Thermochimica Acta, 543*, 150–155, https://doi.org/10.1016/j.tca.2012.05.018

Cerrato, M. E., & Blackmer, A. M. (1990). Comparison of models for describing; corn yield response to nitrogen fertilizer. *Agronomy Journal, 82*(1), 138–143, https://doi.org/10.2134/agronj1990.00021962008200010030x

Chapman, P. M., & Wang, F. (2001). Assessing sediment contamination in estuaries. *Environmental Toxicology and Chemistry, 20*(1), 3–22, https://doi.org/10.1002/etc.5620200102

Cherry, J. A., Shaikh, A. U., Tallman, D. E., & Nicholson, R.v. (1979). Arsenic species as an indicator of redox conditions in groundwater. In *Developments in water science* (Vol. 12, pp. 373–392). Elsevier.

Corzo, M. A. C., Borja-Castro, L. E., Valladares, L. D. L. S., González, J. C., Medina, J. M., Quinde, A. T., Barnes, C. H. W., & Rodriguez, V. A. P. (2022). Magnetic, structural and Mössbauer study of soils from an ancient mining area in Huancavelica-Peru. *Hyperfine Interactions, 243*(1), 3, https://doi.org/10.1007/s10751-021-01786-8

Covey, R. (2006). *How the incas built their heartland*. University of Michigan Press, https://doi.org/10.3998/mpub.88668.

Crompton, T. R. (2001). *Determination of metals and anions in soils, sediments and sludges*. Taylor & Francis Books LTD.

Cullen, W. R., & Reimer, K. J. (1989). Arsenic speciation in the environment. *Chemical Reviews, 89*(4), 713–764.

Dalewski, F. (1999). Removing arsenic from copper smelter gases. *JOM, 51*(9), 24–26, https://doi.org/10.1007/s11837-999-0153-0

Dana, E. S. (1898). *A text-book of mineralogy: with an extended treatise on crystallography and physical mineralogy*. J. Wiley.

Daqing, W. H. W. (1999). Study on surface site types of quartz and calcium carbonate by FDIR spectroscopy. *Journal of Mineralogy and Petrology, 2*.

Davis, A., Ruby, M. v., & Bergstrom, P. D. (1992). Bioavailability of arsenic and lead in soils from the Butte, Montana, mining district. *Environmental Science & Technology, 26*(3), 461–468.

Deer, W. A., Howie, A. R., & Zussman, J. (1966). *An introduction to the rock forming minerals*. John Wiley & Sons.

Dmitrenko, V. V., Dvornyak, A. G., Gratchev, V. M., Kondakova, O. N., Krivova, K. V., Papchenko, A. Y., Sokolov, D. V., Ulin, S. E., Uteshev, Z. M., & Vlasik, K. F. (1999). A thermostable high pressure xenon gamma-ray detector for monitoring concentration of KCl during fertilizer manufacturing. *Nuclear Instruments and Methods in Physics Research Section A: Accelerators, Spectrometers, Detectors and Associated Equipment, 422*(1–3), 326–330, https://doi.org/10.1016/S0168-9002(98)00967-X

Dold, B., Diaby, N., Buselli, E., & Vicetti, R. (2006). *Impact of the construction of a wetland on element mobility in the marine shore porphyry copper tailings deposit, Bahia de Ite, Peru* (Vol. 11). Antofagasta, Chile: Congreso Geológico Chileno., 7-11 Agosto 2006.

Drahota, P., & Filippi, M. (2009). Secondary arsenic minerals in the environment: A review. *Environment International, 35*(8), 1243–1255.

Dumitru, N. T. (1976). *Thermal analysis of minerals*. Abacus Press.

Effeberger, E. L., Mereiter, K., & Zemann, J. (1981). Crystal structure refinements of magnesite, calcite, rhodochrosite, siderite, smithsonite and dolomite with discussion of some aspects of the stereochemistry of calcitc-type carbonates. *Z. Kristallogr, 156*, 233–243.

Eisler, R. (1994). A review of arsenic hazards to plants and animals with emphasis on fishery and wildlife resources. *Advances in Environmental Science and Technology-New York-, 27*, 185.

Elouear, Z., Bouhamed, F., Boujelben, N., & Bouzid, J. (2016). Application of sheep manure and potassium fertilizer to contaminated soil and its effect on zinc, cadmium and lead accumulation by alfalfa plants. *Sustainable Environment Research, 26*(3), 131–135, https://doi.org/10.1016/j.serj.2016.04.004

Eppley, R, W. (1972). Temperature and phytoplankton growth in the sea. *Fishery Bulletin, 70*(4), 1063–1085.

Ettler, V., Johan, Z., Kříbek, B., Veselovský, F., Mihaljevič, M., Vaněk, A., Penížek, V., Majer, V., Sracek, O., & Mapani, B. (2016). Composition and fate of mine-and smelter-derived particles in soils of humid subtropical and hot semi-arid areas. *Science of the Total Environment, 563*, 329–339.

Fernández Massó, L. (2003). *Estudio de mercado sobre fertilizantes en Perú*. http://www.fertilizando.com/estadisticas/estudioMercadoFertilizantesPeru.pdf.

Findoráková, L., Šestinová, O., Danková, Z., Findorák, R., & Hančuľák, J. (2015). Thermal and spectral characterization of bottom sediment from the water reservoir Ružín No. I in Eastern Slovakia and the kinetics of heavy metal cation leaching. *Journal of Soils and Sediments, 15*(8), 1781–1788.

Fischer, R. A., Howe, G. N., & Ibrahim, Z. (1993). Irrigated spring wheat and timing and amount of nitrogen fertilizer. I. Grain yield and protein content. *Field Crops Research, 33*(1–2), 37–56, https://doi.org/10.1016/0378-4290(93)90093-3

Foster, A. L., Brown, G. E., Tingle, T. N., & Parks, G. A. (1998). Quantitative arsenic speciation in mine tailings using X-ray absorption spectroscopy. *American Mineralogist, 83*(5–6), 553–568.

Frink, C. R., Waggoner, P. E., & Ausubel, J. H. (1999). Nitrogen fertilizer: Retrospect and prospect. *Proceedings of the National Academy of Sciences, 96*(4), 1175–1180, https://doi.org/10.1073/pnas.96.4.1175

Frondel, C. (1962). *Dana's system of mineralogy*. Silica Minerals.

Gaál, F., Szöllősy, I., Arnold, M., & Paulik, F. (1994). Determination of the organic matter, metal carbonate and mobile water in soils simultaneous TG, DTG, DTA and EGA techniques. *Journal of Thermal Analysis, 42*(5), 1007–1016, https://doi.org/10.1007/BF02547123

Gail, H.-P., & Sedlmayr, E. (1999). Mineral formation in stellar winds. I. Condensation sequence of silicate and iron grains in stationary oxygen rich outflows. *Astronomy and Astrophysics, 347*, 594–616.

Gallegos-Garcia, M., Ramírez-Muñiz, K., & Song, S. (2012). Arsenic removal from water by adsorption using iron oxide minerals as adsorbents: A review. *Mineral Processing and Extractive Metallurgy Review, 33*(5), 301–315.

Gibbs, G.v. (1977). A study of the structural chemistry of coesite. *Zeitschrift für Kristallographie - Crystalline Materials, 145*(1–6), https://doi.org/10.1524/zkri.1977.145.16.108

Grant, R. W. (1967). New data on tridymite. *American Mineralogist, 52*(3–4), 536–541.

Grzechnik, A. (1999). Compressibility and vibrational modes in solid As4O6. *Journal of Solid State Chemistry, 144*(2), 416–422, https://doi.org/10.1006/jssc.1999.8189

Gudbrandsson, S. (2013). *Experimental weathering rates of aluminium-silicates*. [Université Paul Sabatier - Toulouse III]. https://tel.archives-ouvertes.fr/tel-00933440/file/Thesis_Gudbrandsson.pdf.

Härdter, R., Rex, M., & Orlovius, K. (2005). Effects of different Mg fertilizer sources on the magnesium availability in soils. *Nutrient Cycling in Agroecosystems, 70*(3), 249–259, https://doi.org/10.1007/s10705-005-0408-2

Henke, K. R. (2009). *Environmental chemistry, health threats and waste treatment*. Wiley Online Library.

Please cite this article as: de Los Santos Valladares, L et al., Physical and chemical characterization of sediments from an Andean river exposed to mining and agricultural activities: The Moquegua River, Peru, International Journal of Sediment Research, https://doi.org/10.1016/j.ijsrc.2022.06.002

Huang, C. P., & Fu, P. L. K. (1984). Treatment of arsenic (V)-containing water by the activated carbon process. *Journal (Water Pollution Control Federation)*, 233–242.

Hudson, T. L., Borden, J. C., Russ, M., & Bergstrom, P. D. (1997). Controls on As, Pb, and Mn distribution in community soils of an historical mining district, southwestern Colorado. *Environmental Geology, 33*(1), 25–42.

Hutchins, D. A., Hare, C. E., Weaver, R. S., Zhang, Y., Firme, G. F., DiTullio, G. R., Alm, M. B., Riseman, S. F., Maucher, J. M., Geesey, M. E., Trick, C. G., Smith, G. J., Rue, E. L., Conn, J., & Bruland, K. W. (2002). Phytoplankton iron limitation in the humboldt current and Peru upwelling. *Limnology & Oceanography, 47*(4), 997–1011, https://doi.org/10.4319/lo.2002.47.4.0997

Jaynes, D. B., Colvin, T. S., Karlen, D. L., Cambardella, C. A., & Meek, D. W. (2001). Nitrate loss in subsurface drainage as affected by nitrogen fertilizer rate. *Journal of Environmental Quality, 30*(4), 1305–1314, https://doi.org/10.2134/jeq2001.3041305x

Kazi, T. G., Arain, M. B., Jamali, M. K., Jalbani, N., Afridi, H. I., Sarfraz, R. A., Baig, J. A., & Shah, A. Q. (2009). Assessment of water quality of polluted lake using multivariate statistical techniques: A case study. *Ecotoxicology and Environmental Safety, 72*(2), 301–309, https://doi.org/10.1016/j.ecoenv.2008.02.024

Kempster, C. J. E., Megaw, H. D., & Radoslovich, E. W. (1962). The structure of anorthite, CaAl 2 Si 2 O 8 . I. Structure analysis. *Acta Crystallographica, 15*(10), 1005–1017, https://doi.org/10.1107/S0365110X62002625

Kiiski, H., Dittmar, H., Drach, M., Vosskamp, R., Trenkel, M. E., Gutser, R., & Steffens, G. (2016). Fertilizers, 2. Types. In *Ullmann's encyclopedia of industrial chemistry* (pp. 1–53). Wiley-VCH Verlag GmbH & Co. KGaA, https://doi.org/10.1002/14356007.n10_n01.pub2

Kohl, D. H., Shearer, G. B., & Commoner, B. (1971). Fertilizer nitrogen: Contribution to nitrate in surface water in a corn belt watershed. *Science, 174*(4016), 1331–1334, https://doi.org/10.1126/science.174.4016.1331

Konnert, J. H., & Appleman, D. E. (1978). The crystal structure of low tridymite. *Acta Crystallographica Section B Structural Crystallography and Crystal Chemistry, 34*(2), 391–403, https://doi.org/10.1107/S0567740878003210

Kovac, N., Faganeli, J., Bajt, O., Orel, B., & Vuk, A. (2005). Investigation of sediment samples from the Gulf of Trieste (northern Adriatic) by FTIR spectroscopy. *Mater. Geoenvi., 52*, 81–85.

Kříbek, B., Majer, V., Knésl, I., Keder, J., Mapani, B., Kamona, F., Mihaljevič, M., Ettler, V., Penížek, V., & Vaněk, A. (2016). Contamination of soil and grass in the Tsumeb smelter area, Namibia: Modeling of contaminants dispersion and ground geochemical verification. *Applied Geochemistry, 64*, 75–91.

Ledgard, S. F., Penno, J. W., & Sprosen, M. S. (1999). Nitrogen inputs and losses from clover/grass pastures grazed by dairy cows, as affected by nitrogen fertilizer application. *The Journal of Agricultural Science, 132*(2), 215–225, https://doi.org/10.1017/S002185969800625X

Lengke, M. F., Sanpawanitchakit, C., & Tempel, R. N. (2009). The oxidation and dissolution of arsenic-bearing sulfides. *The Canadian Mineralogist, 47*(3), 593–613, https://doi.org/10.3749/canmin.47.3.593

Liu, C.-W., Lin, K.-H., & Kuo, Y.-M. (2003). Application of factor analysis in the assessment of groundwater quality in a Blackfoot disease area in Taiwan. *Science of the Total Environment, 313*(1–3), 77–89, https://doi.org/10.1016/S0048-9697(02)00683-6

Liu, T.-Y., Chang, C.-Y., & Chiou, T.-J. (2009). The long-distance signaling of mineral macronutrients. *Current Opinion in Plant Biology, 12*(3), 312–319, https://doi.org/10.1016/j.pbi.2009.04.004

Lixian, Y., Xiuchong, Z., Zhiping, P., & Wanzhen, C. (2005). Nutritional characteristics and K and Mg fertilizer combination in Baxi banana. *Plant Nutrition and Fertilizer Science, 11*(Issue 1), 116–121.

Long, G., Peng, Y., & Bradshaw, D. (2012). A review of copper–arsenic mineral removal from copper concentrates. *Minerals Engineering, 36*(38), 179–186, https://doi.org/10.1016/j.mineng.2012.03.032

Lopez-Capel, E., Abbott, G. D., Thomas, K. M., & Manning, D. A. C. (2006). Coupling of thermal analysis with quadrupole mass spectrometry and isotope ratio mass spectrometry for simultaneous determination of evolved gases and their carbon isotopic composition. *Journal of Analytical and Applied Pyrolysis, 75*(2), 82–89, https://doi.org/10.1016/j.jaap.2005.04.004

Macur, R. E., Jackson, C. R., Botero, L. M., Mcdermott, T. R., & Inskeep, W. P. (2004). Bacterial populations associated with the oxidation and reduction of arsenic in an unsaturated soil. *Environmental Science & Technology, 38*(1), 104–111.

Macur, R. E., Wheeler, J. T., McDermott, T. R., & Inskeep, W. P. (2001). Microbial populations associated with the reduction and enhanced mobilization of arsenic in mine tailings. *Environmental Science & Technology, 35*(18), 3676–3682.

Mandal, B. K., & Suzuki, K. T. (2002). Arsenic round the world: A review. *Talanta, 58*(1), 201–235.

Mason, B. (1972). Lunar tridymite and cristobalite. *American Mineralogist, 57*(9–10), 1530–1535.

Matteson, A., & Herron, M. M. (1993). End-member feldspar concentrations determined by FTIR spectral analysis. *Journal of Sedimentary Research, 63*(6), 1144–1148, https://doi.org/10.1306/D4267CC6-2B26-11D7-8648000102C1865D

McKennA, J. (2003). An enhanced cluster analysis program with bootstrap significance testing for ecological community analysis. *Environmental Modelling & Software, 18*(3), 205–220, https://doi.org/10.1016/S1364-8152(02)00094-4

Mecozzi, R., Palma, L. di, & Filippis, P. de (2008). Effect of modified Fenton treatment on the thermal behavior of contaminated harbor sediments. *Chemosphere, 71*(5), 843–852, https://doi.org/10.1016/j.chemosphere.2007.11.034

Megaw, H. D., Kempster, C. J. E., & Radoslovich, E. W. (1962). The structure of anorthite, CaAl 2 Si 2 O 8 . II. Description and discussion. *Acta Crystallographica, 15*(10), 1017–1035, https://doi.org/10.1107/S0365110X62002637

Mok, W. M. (1994). Mobilization of arsenic in contaminated river waters & Removal of arsenic in drinking water treatment. *Arsenic in the Environment. Part 1: Cycling and Characterization*, 99–132.

Nazari, A. M., Radzinski, R., & Ghahreman, A. (2017). Review of arsenic metallurgy: Treatment of arsenical minerals and the immobilization of arsenic. *Hydrometallurgy, 174*, 258–281, https://doi.org/10.1016/j.hydromet.2016.10.011

Nesbitt, H. W., & Muir, I. J. (1998). Oxidation states and speciation of secondary products on pyrite and arsenopyrite reacted with mine waste waters and air. *Mineralogy and Petrology, 62*(1), 123–144.

Nichols, J. T., Reece, P. E., Hergert, G. W., & Moser, L. E. (1990). Yield and quality response of subirrigated meadow vegetation to nitrogen, phosphorus and sulfur fertilizer. *Agronomy Journal, 82*(1), 47–52, https://doi.org/10.2134/agronj1990.00021962008200010010x

Ondrus, P., Veselovsky, F., Hlousek, J., Skala, R., Vavrin, I., Fryda, J., Cejka, J., & Gabasova, A. (1997). Secondary minerals of the Jáchymov (Joachimsthal) ore district. *Journal of Geosciences, 42*(4), 3–76.

Otto, M. (1998). Multivariate methods. *Analytical Chemistry*, 916.

Oudghiri Idrissi Youssefi, F., García-Morales, J. L., & Rodríguez-Barroso, M. (2015). Evaluation of sediments decontamination by chelating agents using thermogravimetric analysis. *International Journal of Environmental Research, 9*, 657–662.

Oudghiri, F., García-Morales, J. L., & Rodríguez-Barroso, M. R. (2014). Rapid screening of estuarine sediments properties using thermogravimetric analysis and attenuated total reflectance (ATR) by fourier transform infrared (FTIR) spectrometry. *Water, Air, & Soil Pollution, 225*(2), 1853, https://doi.org/10.1007/s11270-013-1853-1

Oudghiri, F., García-Morales, J. L., & Rodríguez-Barroso, M. R. (2015). Novel use of TGA–FTIR technique to predict the pollution degree in marine sediments. *Infrared Physics & Technology, 72*, 52–57, https://doi.org/10.1016/j.infrared.2015.07.006

le Page, Y., & Donnay, G. (1976). Refinement of the crystal structure of low-quartz. *Acta Crystallographica Section B Structural Crystallography and Crystal Chemistry, 32*(8), 2456–2459, https://doi.org/10.1107/S0567740876007966

Paktunc, D., Foster, A., Heald, S., & Laflamme, G. (2004). Speciation and characterization of arsenic in gold ores and cyanidation tailings using X-ray absorption spectroscopy. *Geochimica et Cosmochimica Acta, 68*(5), 969–983.

Palacios, P. R., Bustamante, A., de Los Santos Valladares, L., & Gonzalez, J. C. (2012). Study of the dehydroxylation in the hydrated ferric oxide named limonite. *Revista de la Sociedad Quimica del Peru, 78*(3), 198–207.

Pereira, M. de G., de Andrade, M. V. A. S., Ornelas, V. C., de Almeida, R. A. N., Fontes, M. P. F., Ribeiro, J. N., Ribeiro, A. V. F. N., dos Santos, A. V., Souza, A. N., de Araújo, C. B., de Araújo, A. C. B., Onofre, C. R. E., & Korn, M. das G. A. (2012). Assessment of physical-chemical characteristics of water and sediments from a Brazilian Tropical estuary: Status and environmental implications. *The Scientific World Journal*, 1–14, https://doi.org/10.1100/2012/676173, 2012.

Perera, D. H. N., Arvidsson-Shukur, D. R. M., Barnes, E. P. G., Newton, P. J., Pacheco, E. E., Byrne, P., Valladares, L. D. L. S., & Barnes, C. H. W. (2021). *Water quality dynamics in a hyper-arid Andean river basin subject to large-scale mining and agricultural activities: The Moquegua River system in southern Peru*.

Pertlik, F. (1978). Structure refinement of cubic As_2O_3 (arsenolithe) with single-crystal data. *Proc. J. Phys., 28*, 170–176.

Piret, N. L. (1999). The removal and safe disposal of arsenic in copper processing. *JOM, 51*(9), 16–17, https://doi.org/10.1007/s11837-999-0150-3

Plante, A. F., Pernes, M., & Chenu, C. (2005). Changes in clay-associated organic matter quality in a C depletion sequence as measured by differential thermal analyses. *Geoderma, 129*(3), 186–199, https://doi.org/10.1016/j.geoderma.2004.12.043

Pluth, J. J., Smith, J. v, & Faber, J. (1985). Crystal structure of low cristobalite at 10, 293, and 473 K: Variation of framework geometry with temperature. *Journal of Applied Physics, 57*(4), 1045–1049, https://doi.org/10.1063/1.334545

Prakash, S., & Verma, J. P. (2016). Global perspective of potash for fertilizer production. In *Potassium solubilizing microorganisms for sustainable agriculture* (pp. 327–331). Springer India, https://doi.org/10.1007/978-81-322-2776-2_23

Ramasamy, V., Rajkumar, P., & Ponnusamy, V. (2009). Depth wise analysis of recently excavated Vellar river sediments through FTIR and XRD studies. *Indian Journal of Physics, 83*(9), 1295–1308, https://doi.org/10.1007/s12648-009-0110-3

Rangkadilok, N., Nicolas, M. E., Bennett, R. N., Eagling, D. R., Premier, R. R., & Taylor, P. W. J. (2004). The effect of sulfur fertilizer on glucoraphanin levels in broccoli (B. oleracea L. var. italica) at different growth stages. *Journal of Agricultural and Food Chemistry, 52*(9), 2632–2639, https://doi.org/10.1021/jf030655u

Reig, F. (2002). FTIR quantitative analysis of calcium carbonate (calcite) and silica (quartz) mixtures using the constant ratio method. Application to geological samples. *Talanta, 58*(4), 811–821, https://doi.org/10.1016/S0039-9140(02)00372-7

Rice, P. M. (1994). The kilns of Moquegua, Peru: Technology, excavations, and functions. *Journal of Field Archaeology, 21*(3), 325–344, https://doi.org/10.1179/009346994791547599

Rickwood, P. C. (1981). The largest crystals. *American Mineralogist, 66*(9–10), 885–907.

Rodríguez-Barroso, M. R., Solar, M. R., Blanco, E., Quiroga, J. M., & García-Morales, J. L. (2006). Thermal analysis in the evaluation of sediment pollution. *Environmental Technology, 27*(9), 1001–1009, https://doi.org/10.1080/09593332708618708

Ross, N. L., Shu, J., & Hazen, R. M. (1990). High-pressure crystal chemistry of stishovite. *American Mineralogist, 75*(7–8), 739–747.

Please cite this article as: de Los Santos Valladares, L et al., Physical and chemical characterization of sediments from an Andean river exposed to mining and agricultural activities: The Moquegua River, Peru, International Journal of Sediment Research, https://doi.org/10.1016/j.ijsrc.2022.06.002

Rotting, T., Amezaga, J., Younger, P., Jimenez, P., Talavera, C., Quintanilla, J., Oyarzún, R., & Soto, G. (2009). Catchment management and mining impacts in arid and semi-arid South America (CAMINAR): Case studies in Peru, Bolivia and Chile. In *8th international conference on acid rock drainage (ICARD) and securing the future: Mining, metals & the environment in a sustainable society 2009*.

Rowell, D. L. (1994). *Soil science*. Routledge, https://doi.org/10.4324/9781315844855.

Rowland, R. A. (1952). Differential thermal analysis of clays and carbonates. *Clays and Clay Minerals, 1*(1), 151–163, https://doi.org/10.1346/CCMN.1952.0010118

Scanavino, I., Belousov, R., & Prencipe, M. (2012). Ab initio quantum-mechanical study of the effects of the inclusion of iron on thermoelastic and thermodynamic properties of periclase (MgO). *Physics and Chemistry of Minerals, 39*(8), 649–663, https://doi.org/10.1007/s00269-012-0519-7

Scarpelli, W. (2005). Arsenic in the rivers of the amazon basin. *Terra, 2*(1–2), 20–27.

Schnitzer, M., Turner, R. C., & Hoffman, I. (1964). A thermogravimetric study of organic matter of representative canadian podzol soils. *Canadian Journal of Soil Science, 44*(1), 7–13, https://doi.org/10.4141/cjss64-002

Sclar, C. B., Carrison, L. C., & Schwartz, C. M. (1962). Optical crystallography of coesite. *American Mineralogist, 47*(11–12), 1292–1302.

Shibayama, A., Takasaki, Y., William, T., Yamatodani, A., Higuchi, Y., Sunagawa, S., & Ono, E. (2010). Treatment of smelting residue for arsenic removal and recovery of copper using pyro–hydrometallurgical process. *Journal of Hazardous Materials, 181*(1–3), 1016–1023.

Sihuas, N. (2016). *Boletín estadístico de medios de producción agropecuarios, Ministerios de Agricultura y Riego*. http://minagri.gob.pe/portal/download/pdf/herramientas/boletines/prod-agropecuarios/2016/boletin-estad-medios-produccion-agropec-feb16.pdf.

Sims, K. (2010). After state collapse. *After Collapse: The Regeneration of Complex Societies*, 114.

Sinclair, W., & Ringwood, A. E. (1978). Single crystal analysis of the structure of stishovite. *Nature, 272*(5655), 714–715, https://doi.org/10.1038/272714a0

Šlejkovec, Z., Falnoga, I., & van Elteren, J. T. (2012). Arsenic trioxide versus tetraarsenic oxide in biomedical research: Misunderstandings and misinterpretations. *Biometals, 25*(1), 231–235.

Smyth, J. R., & Hatton, C. J. (1977). A coesite-sanidine grospydite from the Roberts Victor kimberlite. *Earth and Planetary Science Letters, 34*(2), 284–290, https://doi.org/10.1016/0012-821X(77)90012-7

Sohi, S. P., Mahieu, N., Arah, J. R. M., Powlson, D. S., Madari, B., & Gaunt, J. L. (2001). A procedure for isolating soil organic matter fractions suitable for modeling. *Soil Science Society of America Journal, 65*(4), 1121–1128, https://doi.org/10.2136/sssaj2001.6541121x

Sohrin, Y., Matsui, M., Kawashima, M., Hojo, M., & Hasegawa, H. (1997). Arsenic biogeochemistry affected by eutrophication in Lake Biwa, Japan. *Environmental Science & Technology, 31*(10), 2712–2720.

Sokal, R. R., & Rohlf, F. J. (1962). The comparison of dendrograms by objective methods. *Taxon, 11*(2), 33–40, https://doi.org/10.2307/1217208

Southern Copper Corporation. (2015). *Formulary 10-K from 2015, annual report of agreement with the stipulated in section of the stock exchange of 1934 for the fiscal exercise which finished at December 31st, 2015. Commission file number 1-14066* http://www.southernperu.com/esp/relinv/2015/10K/10K2015e.pdf

Sternberg, L. da S. L., Pinzon, M. C., Moreira, M. Z., Moutinho, P., Rojas, E. I., & Herre, E. A. (2007a). Plants use macronutrients accumulated in leaf-cutting ant nests. *Proceedings of the Royal Society B: Biological Sciences, 274*(1608), 315–321, https://doi.org/10.1098/rspb.2006.3746

Sternberg, L. da S. L., Pinzon, M. C., Moreira, M. Z., Moutinho, P., Rojas, E. I., & Herre, E. A. (2007b). Plants use macronutrients accumulated in leaf-cutting ant nests. *Proceedings of the Royal Society B: Biological Sciences, 274*(1608), 315–321, https://doi.org/10.1098/rspb.2006.3746

Steurer, W., & Jagodzinski, H. (1988). The incommensurately modulated structure of an andesine (An 38). *Acta Crystallographica Section B Structural Science, 44*(4), 344–351, https://doi.org/10.1107/S0108768188001806

Tang, C., Zhu, J., Li, Z., Zhu, R., Zhou, Q., Wei, J., He, H., & Tao, Q. (2015). Surface chemistry and reactivity of SiO2 polymorphs: A comparative study on α-quartz and α-cristobalite. *Applied Surface Science, 355*, 1161–1167, https://doi.org/10.1016/j.apsusc.2015.07.214

Tenorio, G. E., Vanacker, V., Campforts, B., Álvarez, L., Zhiminaicela, S., Vercruysse, K., Molina, A., & Govers, G. (2018). Tracking spatial variation in river load from Andean highlands to inter-Andean valleys. *Geomorphology, 308*, 175–189, https://doi.org/10.1016/j.geomorph.2018.02.009

Tessier, A., Campbell, P. G. C., & Bisson, M. (1979). Sequential extraction procedure for the speciation of particulate trace metals. *Analytical Chemistry, 51*(7), 844–851, https://doi.org/10.1021/ac50043a017

Tironi, A., Trezza, M. A., Irassar, E. F., & Scian, A. N. (2012). Thermal treatment of kaolin: Effect on the pozzolanic activity. *Procedia Materials Science, 1*, 343–350, https://doi.org/10.1016/j.mspro.2012.06.046

Treacy, D. J., & Taylor, P. C. (1981). Nuclear quadrupole resonance in two crystalline forms of As2O3, Arsenolite and Claudetite I. *Solid State Communications, 40*(2), 135–138.

Tuttle, O. F., & Bowen, N. L. (1950). High-temperature albite and contiguous feldspars. *The Journal of Geology, 58*(5), 572–583, https://doi.org/10.1086/625763

Uebel, E., & Heinsdorf, D. (1997). Results of long-term K and Mg fertilizer experiments in afforestation. *Forest Ecology and Management, 91*(1), 47–52, https://doi.org/10.1016/S0378-1127(96)03882-0

Utsunomiya, S., Peters, S. C., Blum, J. D., & Ewing, R. C. (2003). Nanoscale mineralogy of arsenic in a region of New Hampshire with elevated As-concentrations in the groundwater. *American Mineralogist, 88*(11–12), 1844–1852.

de Vries, T. J., & Schrader, H. (1981). Variation of upwelling/oceanic conditions during the latest pleistocene through holocene off the central Peruvian coast: A diatom record. *Marine Micropaleontology, 6*(2), 157–167, https://doi.org/10.1016/0377-8398(81)90003-7

Wang, Q., Li, Y., & Wang, Y. (2011). Optimizing the weight loss-on-ignition methodology to quantify organic and carbonate carbon of sediments from diverse sources. *Environmental Monitoring and Assessment, 174*(1), 241–257, https://doi.org/10.1007/s10661-010-1454-z

Webb, D. A. (1939). The sodium and potassium content of sea water. *Journal of Experimental Biology, 16*(2), 178–183.

Weisenberg, I. J., Bakshi, P. S., & Vervaert, A. E. (1979). Arsenic distribution and control in copper smelters. *JOM, 31*(10), 38–44, https://doi.org/10.1007/BF03354510

Wennemer, M., & Thompson, A. B. (1984). Tridymite polymorphs and polytypes. *Schweizerische Mineralogische Und Petrographische Mitteilungen, 64*(3), 335–353.

Wen, G., Schoenau, J. J., Yamamoto, T., & Inoue, M. (2001). A model of oxidation of an elemental sulfur fertilizer in soils. *Soil Science, 166*(9).

Williams, M., Fordyce, F., Paijitprapapon, A., & Charoenchaisri, P. (1996). Arsenic contamination in surface drainage and groundwater in part of the southeast Asian tin belt, Nakhon Si Thammarat Province, southern Thailand. *Environmental Geology, 27*(1), 16–33.

Wisniak, J., & Garces, I. (2001). *The rise and fall of the salitre (sodium nitrate) industry*.

Wooding, A. R., Kavale, S., MacRitchie, F., Stoddard, F. L., & Wallace, A. (2000). Effects of nitrogen and sulfur fertilizer on protein composition, mixing requirements, and dough strength of four wheat cultivars. *Cereal Chemistry Journal, 77*(6), 798–807, https://doi.org/10.1094/CCHEM.2000.77.6.798

Yamazaki, D., Yoshino, T., Matsuzaki, T., Katsura, T., & Yoneda, A. (2009). Texture of (Mg,Fe)SiO3 perovskite and ferro-periclase aggregate: Implications for rheology of the lower mantle. *Physics of the Earth and Planetary Interiors, 174*(1–4), 138–144, https://doi.org/10.1016/j.pepi.2008.11.002

Yang, B., Zhang, G. L., Deng, W., & Ma, J. (2013). Review of arsenic pollution and treatment progress in nonferrous metallurgy industry. *Advanced Materials Research, 634*, 3239–3243.

Zhu, Z. L., & Chen, D. L. (2002). Nitrogen fertilizer use in China – contributions to food production, impacts on the environment and best management strategies. *Nutrient Cycling in Agroecosystems, 63*(2), 117–127, https://doi.org/10.1023/A:1021107026067

Please cite this article as: de Los Santos Valladares, L et al., Physical and chemical characterization of sediments from an Andean river exposed to mining and agricultural activities: The Moquegua River, Peru, International Journal of Sediment Research, https://doi.org/10.1016/j.ijsrc.2022.06.002